Geophys. J. Int. (2011) **187,** 1645–1667 doi: 10.1111/j.1365-246X.2011.05221.x

3-D finite-difference, finite-element, discontinuous-Galerkin and spectral-element schemes analysed for their accuracy with respect to *P*-wave to *S*-wave speed ratio

Peter Moczo,[1,2] Jozef Kristek,[1,2] Martin Galis,[1,2] Emmanuel Chaljub[3] and Vincent Etienne[4]

[1] *Faculty of Mathematics, Physics and Informatics, Comenius University Bratislava, Mlynska dolina F1, 84248 Bratislava, Slovak Republic. E-mail: moczo@fmph.uniba.sk*
[2] *Geophysical Institute, Slovak Academy of Sciences, Dubravska cesta* 9, 84528 *Bratislava, Slovak Republic*
[3] *ISTerre, Université Joseph Fourier, BP* 53, 38041 *Grenoble, France*
[4] *Géoazur,* 250 *rue Albert Einstein, Sophia Antipolis,* 06560 *Valbonne, France*

Accepted 2011 September 5. Received 2011 August 15; in original form 2011 April 19

SUMMARY

We analyse 13 3-D numerical time-domain explicit schemes for modelling seismic wave propagation and earthquake motion for their behaviour with a varying *P*-wave to *S*-wave speed ratio (V_P/V_S). The second-order schemes include three finite-difference, three finite-element and one discontinuous-Galerkin schemes. The fourth-order schemes include three finite-difference and two spectral-element schemes. All schemes are second-order in time. We assume a uniform cubic grid/mesh and present all schemes in a unified form. We assume plane *S*-wave propagation in an unbounded homogeneous isotropic elastic medium. We define relative local errors of the schemes in amplitude and the vector difference in one time step and normalize them for a unit time. We also define the equivalent spatial sampling ratio as a ratio at which the maximum relative error is equal to the reference maximum error. We present results of the extensive numerical analysis.

We theoretically (i) show how a numerical scheme sees the *P* and *S* waves if the V_P/V_S ratio increases, (ii) show the structure of the errors in amplitude and the vector difference and (iii) compare the schemes in terms of the truncation errors of the discrete approximations to the second mixed and non-mixed spatial derivatives.

We find that four of the tested schemes have errors in amplitude almost independent on the V_P/V_S ratio.

The homogeneity of the approximations to the second mixed and non-mixed spatial derivatives in terms of the coefficients of the leading terms of their truncation errors as well as the absolute values of the coefficients are key factors for the behaviour of the schemes with increasing V_P/V_S ratio.

The dependence of the errors in the vector difference on the V_P/V_S ratio should be accounted for by a proper (sufficiently dense) spatial sampling.

Key words Numerical approximations and analysis; Computational seismology; Theoretical seismology.

1 INTRODUCTION

When numerically modelling seismic wave propagation and earthquake ground motion in a local or regional scale, we often consider a finite volume of the Earth. Typically, the volume has a shape of a cuboid (a rectangular parallelepiped) with the top face representing a flat free surface and other faces representing transparent boundaries or planes of symmetry. In a more realistic case, the free Earth's surface has a non-planar topography. The medium inside is often considered a heterogeneous isotropic viscoelastic continuum. If we cover the computational domain by a space–time grid of points or elements, then the overall accuracy of the numerical modelling for the given space–time discretization and source–receiver configuration may depend on some or all of the following factors:

(1) accuracy in
  (i) a homogeneous medium (V_P/V_S—*P*-wave to *S*-wave speed ratio)
  (ii) a smoothly spatially varying medium (spatial variability of material parameters)
(2) accuracy at
  (i) a material interface (geometry, continuity of displacement and traction)
  (ii) a free surface (geometry, zero traction)
(3) accuracy of
  (i) a grid boundary (transparency or symmetry)
  (ii) simulation of source (location, mechanism, time function)
  (iii) incorporation of attenuation (frequency dependence, spatial variability)

Articles presenting numerical methods or schemes usually include and some of them focus first of all on the stability and grid dispersion in an unbounded homogeneous medium. This is fundamental and necessary. Not all articles sufficiently address the other factors determining the overall accuracy of the numerical modelling. Surprisingly enough, the least attention has been paid to the accuracy with respect to the V_P/V_S ratio.

At the same time, in surface sediments, and mainly in sedimentary basins and valleys, the ratio V_P/V_S is often as large as five or more (e.g. larger than 10 in the unconsolidated lake sediments in Ciudad de México). Recent numerical-modelling exercises focused on the deep Alpine sediment valley beneath Grenoble, France and the sedimentary Mygdonian Basin near Thessaloniki, Greece (e.g. Chaljub *et al*. 2010a,b; Moczo *et al*. 2010a), also confirm the necessity to account for large V_P/V_S ratios with sufficient accuracy.

Moczo *et al*. (2010b) investigated accuracy of four finite-difference (FD) and three finite-element (FE) schemes with respect to the V_P/V_S ratio. Their investigation was restricted to the basic second-order 2-D schemes. They aimed to identify and select the very basic inherent aspects of the schemes responsible for their behaviour with respect to the varying V_P/V_S ratio, and to compare different schemes at the most fundamental level. They indicated that consistency in approximating first spatial derivatives and, consequently, the second mixed and non-mixed spatial derivatives appears to be the key factor for the behaviour of a scheme with respect to the V_P/V_S ratio.

Moczo *et al*. (2010b) introduced the problem of the accuracy with respect to the V_P/V_S ratio in sufficient extent and detail. Therefore, we do not repeat here the extensive introduction and rather refer readers to the latter paper.

In this paper, we focus on investigating the accuracy of 3-D time-domain explicit numerical schemes of second-order in time and second- and fourth-order in space with respect to the V_P/V_S ratio in an unbounded homogeneous medium. We include schemes based on the FD, FE, spectral-element (SE) and discontinuous-Galerkin (DG) methods.

We present all the investigated schemes in a unified form and define (full) local errors in one time integration step. Because different schemes use different time steps (according to appropriate stability conditions), we normalize the errors with respect to time. Consequently, we can directly compare numerically evaluated errors of different schemes. We perform extensive numerical analysis for wide ranges of values of the V_P/V_S ratio and spatial sampling ratio, and for the entire range of directions of propagation with respect to the spatial grid. We analyse and interpret the numerical results in terms of the inherent structures of the numerical schemes. We eventually develop general conclusions on the accuracy of the numerical schemes with respect to the V_P/V_S ratio and on the numerical efficiency of the schemes in practical applications.

2 EQUATIONS OF MOTION FOR A HOMOGENEOUS MEDIUM

Consider a Cartesian coordinate system (x, y, z) and an unbounded homogeneous perfectly elastic isotropic medium. Let ρ denote density, λ and μ Lamé elastic moduli, $\alpha = [(\lambda + 2\mu)/\rho]^{1/2}$ and $\beta = (\mu/\rho)^{1/2}$ *P*-wave and *S*-wave speeds (i.e. V_P and V_S). Let displacement components $u_i \; ; \; i \in \{x, y, z\}$ and stress-tensor components $\sigma_{ij} \; ; \; i, j \in \{x, y, z\}$ be functions of the spatial coordinates and time t. Denote

$$\varphi_{,\xi} = \frac{\partial \varphi}{\partial \zeta}; \quad \varphi \in \{u_i, \; \sigma_{ij}\}, \quad i, j \in \{x, y, z\}, \quad \zeta \in \{t, x, y, z\}. \tag{1}$$

We will consider two strong forms of the equation of motion without the body force term. The displacement-stress (DS) formulation of the equation of motion is

$$\begin{aligned}
\rho u_{x,tt} &= \sigma_{xx,x} + \sigma_{xy,y} + \sigma_{xz,z} \\
\rho u_{y,tt} &= \sigma_{yy,y} + \sigma_{yz,z} + \sigma_{yx,x} \\
\rho u_{z,tt} &= \sigma_{zz,z} + \sigma_{zx,x} + \sigma_{zy,y}
\end{aligned} \tag{2}$$

$$\begin{aligned}
\sigma_{xx} &= (\lambda + 2\mu) u_{x,x} + \lambda u_{y,y} + \lambda u_{z,z} \\
\sigma_{yy} &= (\lambda + 2\mu) u_{y,y} + \lambda u_{z,z} + \lambda u_{x,x} \\
\sigma_{zz} &= (\lambda + 2\mu) u_{z,z} + \lambda u_{x,x} + \lambda u_{y,y} \\
\sigma_{xy} &= \mu \, (u_{x,y} + u_{y,x}) \\
\sigma_{yz} &= \mu \, (u_{y,z} + u_{z,y}) \\
\sigma_{zx} &= \mu \, (u_{z,x} + u_{x,z}).
\end{aligned} \tag{3}$$

The displacement (D) formulation is

$$\rho u_{x,tt} = (\lambda + 2\mu)u_{x,xx} + \lambda\,(u_{y,yx} + u_{z,zx}) + \mu\,(u_{x,yy} + u_{y,xy} + u_{z,xz} + u_{x,zz})$$
$$\rho u_{y,tt} = (\lambda + 2\mu)u_{y,yy} + \lambda\,(u_{z,zy} + u_{x,xy}) + \mu\,(u_{y,zz} + u_{z,yz} + u_{x,yx} + u_{y,xx})$$
$$\rho u_{z,tt} = (\lambda + 2\mu)u_{z,zz} + \lambda\,(u_{x,xz} + u_{y,yz}) + \mu\,(u_{z,xx} + u_{x,zx} + u_{y,zy} + u_{z,yy}). \quad (4)$$

Eqs (4) can be written as

$$u_{x,tt} = \alpha^2(u_{x,xx} + u_{y,yx} + u_{z,zx}) + \beta^2\,(u_{x,yy} - u_{y,yx} + u_{x,zz} - u_{z,zx})$$
$$u_{y,tt} = \alpha^2(u_{y,yy} + u_{z,zy} + u_{x,xy}) + \beta^2\,(u_{y,zz} - u_{z,zy} + u_{y,xx} - u_{x,xy})$$
$$u_{z,tt} = \alpha^2(u_{z,zz} + u_{x,xz} + u_{y,yz}) + \beta^2\,(u_{z,xx} - u_{x,xz} + u_{z,yy} - u_{y,yz}). \quad (5)$$

The weak form of the equation of motion (e.g. Zienkiewicz & Taylor 1989; Hughes 2000; Moczo *et al*. 2007a) is

$$\int_\Omega w\,(\rho\,u_{i}{}_{,tt})\,\mathrm{d}\Omega + \int_\Omega w_{,k}\;\sigma_{ik}\,\mathrm{d}\Omega - \int_{\Gamma_N} w\,h_i\,\mathrm{d}\Gamma = 0, \quad (6)$$

where Ω is a volume of a medium with boundary Γ, h_i is a prescribed traction on part Γ_N of boundary Γ and the equations have to be satisfied for all possible choices of weight functions w.

3 NUMERICAL SCHEMES

Several numerical methods can be used to solve the strong-form and weak-form equations of motion. The analysis by Moczo *et al*. (2010b) was restricted to the basic 2-D second-order FD and FE schemes. Here, we investigate 13 3-D time-domain numerical schemes of second- and fourth-order in space based on four important numerical methods—FD, FE, DG and SE methods. We use three uniform spatial grids in the FD schemes—conventional, partly-staggered and staggered (Fig. 1a). The other schemes are constructed on the mesh of uniform cubic elements. The elements considered for the FE and SE schemes are illustrated in Figs 1(b) and (c), respectively. All schemes are explicit and second-order accurate in time. The choice of the explicit schemes well reflects the fact that the explicit schemes are strongly dominant in recent numerical modelling of seismic wave propagation and earthquake ground motion. The same is true about the second-order accuracy in time. The powerful and sophisticated ADER-DG method (Arbitrary high-order DERivative Discontinuous Galerkin, for details see Section 3.3) makes a significant exception. We do not include possible ADER-DG of higher order because so far they have been developed for tetrahedral grids, and the higher order in time would have no comparison among the other schemes.

Given the variety of methods, grids, approximation orders and integrations in elements, we have to introduce easy-to-follow acronyms to be used throughout the paper.

An acronym of each investigated scheme starts with two letters indicating a method. FD stands for the finite-difference method. Similarly, FE, DG or SE indicate the finite-element, discontinuous-Galerkin or spectral-element method, respectively.

The FD schemes differ from each other by the equation formulation, grid and order of approximation. D indicates the displacement formulation, DS the displacement-stress formulation. CG indicates conventional grid, PSG partly-staggered grid, and SG staggered grid. 2 or 4 indicates the second- or fourth-order approximation in space. The lower-case 'a' or 'b' indicates one of two variants of the fourth-order approximation. The acronyms of the six considered schemes are FD D CG 2, FD DS PSG 2, FD DS SG 2, FD D CG 4a, FD D CG 4b and FD DS SG 4.

All three of the FE schemes considered solve the weak-form of the equation of motion on the mesh of uniform cubic elements and are second-order accurate in space. The schemes differ in the integration applied within an element. Consequently, the method indicator is followed by the indicator of the integration. L8, G1 or G8 indicates Lobatto 8-point, Gauss 1-point or Gauss 8-point integration, respectively. The acronyms of the three considered schemes are FE L8, FE G1 and FE G8.

In the case of the DG schemes, we explicitly indicate the polynomial degree of the basis functions, P0 or P1, and the centred flux, CF, to clearly distinguish the schemes from a large variety of possible DG schemes. The acronyms are DG P0 CF and DG P1 CF.

The order of approximation is explicitly indicated for two SE schemes. Indicators cn and vn then distinguish the central node and vertex node. The acronyms are SE 4 cn and SE 4 vn.

The acronyms and essential characteristics of all 13 considered numerical schemes are given in Fig. 2.

3.1 The finite-difference schemes

Reviews of the FD schemes on the conventional, partly-staggered and staggered grids, including original references, can be found, for example, in extensive texts by Moczo *et al*. (2007a,b).

3.1.1 FD D CG 2, FD D CG 4a, FD D CG 4b

FD D CG 2, the second-order FD scheme solving the strong-form equation of motion for displacement on the conventional grid, is obtained if derivatives in eqs (5) are replaced using standard second-order centred FD formulae approximating second non-mixed and mixed derivatives.

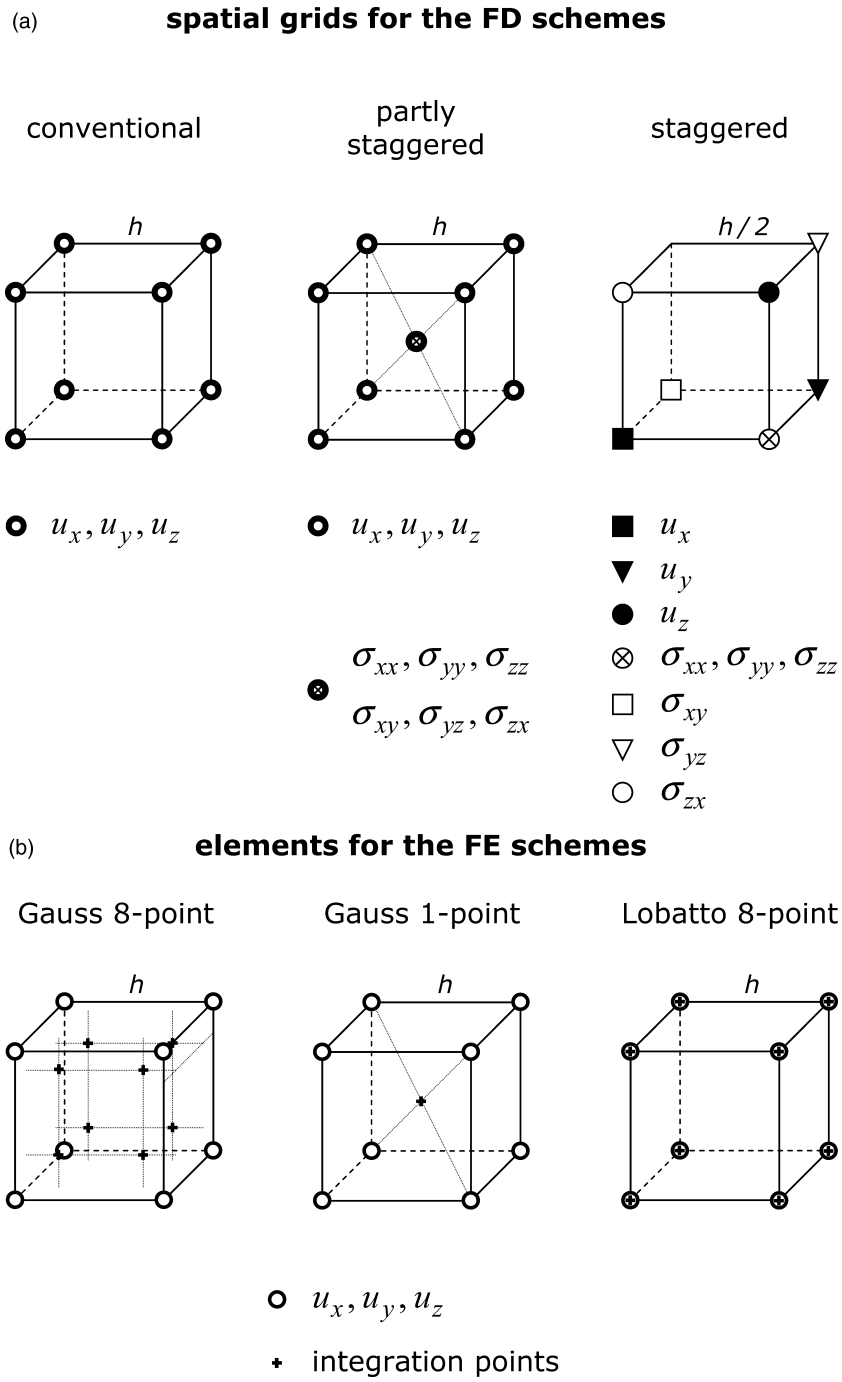

Figure 1. (a) Spatial grids for the FD schemes considered in this study. Left-hand panel: conventional grid-–all displacement components are located at each grid point (position). Centre panel: partly-staggered grid—all displacement components share the same grid points whereas all stress-tensor components share other grid points. Right-hand panel: staggered grid—each of the quantities has its own grid position except the normal stress-tensor components sharing one grid position. (b) The cubic element used for the FE schemes. The nodal points are represented by empty circles. The integration points used in the Gauss 8-point, Gauss 1-point and Lobatto 8-point integrations are represented by crosses. The integration points in the Gauss 8-point integration define vertices of a centred cube with the edge equal to $2h/\sqrt{3}$. The positions of the other integration points are obvious. (c) The cubic element used for the SE schemes. The nodal points are also the integration points. The vertex and central nodes are explicitly indicated by empty circles. For the positions of the nodal points we refer to Chaljub *et al*. (2007).

On the conventional grid, we can find several fourth-order approximations to the second non-mixed and mixed spatial derivatives. Therefore, we include two different approximations to the second non-mixed and mixed spatial derivatives and, thus, two different schemes. Based on the indication found by Moczo *et al*. (2010b), we constructed one scheme with the minimum possible equal coefficients of the leading terms of the truncation errors for the mixed and non-mixed derivatives—FD D CG 4a. The other scheme, FD D CG 4b, has the minimum possible spatial stencil and a relatively large difference between values of coefficients of the leading terms of the truncation errors.

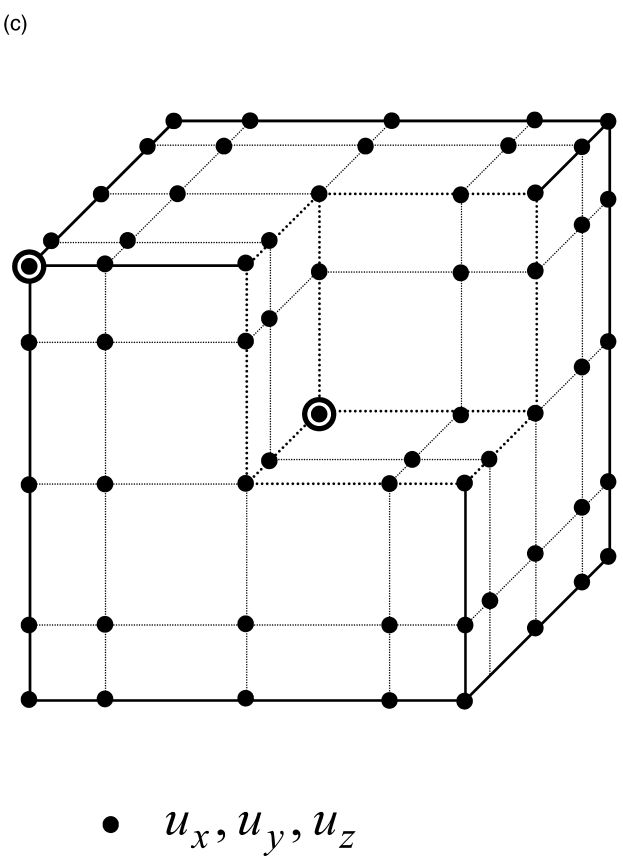

Figure 1. (*Continued.*)

3.1.2 FD DS SG 2, FD DS SG 4

FD DS SG 2 is obtained in the following way: The second time derivatives in eqs (2) are replaced using the standard second-order centred FD formula approximating the second derivative. The first spatial derivatives of the stress-tensor components in eqs (2) are replaced using the standard second-order centred FD formula approximating the first derivative. Then, all discrete stress-tensor components on the right-hand side (r.h.s.) of the obtained schemes are replaced by their FD approximations. The approximations are obtained from eqs (3), in which the first derivatives are replaced using the standard second-order centred FD formula approximating the first derivative. In the resulting final scheme only displacement components appear. This is important to note, given the fact that the scheme solves the DS formulation of the equation of motion on the staggered grid. Note that this type of scheme is also called the parsimonious scheme.

FD DS SG 4 is obtained in the same way except that fourth-order FD approximations are used to replace the first spatial derivatives of the stress-tensor and displacement components.

3.1.3 FD DS PSG 2

For comparison with FD D CG 2 and FD DS SG 2, we also include the second-order scheme solving the DS formulation of the equation of motion on the partly-staggered grid. The scheme is obtained in the same way as FD S SG 2 except that the FD approximations are more complicated. The complication is due to the fact that the stress-tensor components are displaced from the displacement components by a half-grid spacing in all three Cartesian directions (see Fig. 1). For example, in approximating the x-derivative of the stress-tensor component at a grid position of the displacement component, the required values of the stress-tensor components are obtained as arithmetic averages of the values at four stress-tensor component grid positions in the corresponding yz-grid planes.

We do not include the velocity–stress (VS) staggered grid schemes. They differ from the FD DS SG schemes only in approximating time derivatives. They approximate second spatial derivatives of the particle-velocity components (in the resulting final schemes) in the same way as the FD DS SG schemes approximate the second spatial derivatives of the displacement components. Moczo *et al*. (2010b) showed that the difference between the behaviours of the corresponding 2-D schemes with respect to the V_P/V_S ratio due to different time derivatives is negligible. Conclusions for the FD VS SG schemes related to the approximations to the spatial derivatives are the same as those for the FD DS SG schemes.

3D numerical schemes					
method		**equation formulation**	**grid**	**add. specif.**	**order**
FD D CG 2	finite-difference	displacement	conventional		2
FD DS PSG 2		displacement-stress	partly-staggered		
FD DS SG 2		displacement-stress	staggered		
FE L8	finite-element	displacement	conventional	Lobatto 8-point integr.	
FE G1				Gauss 1-point integr.	
FE G8				Gauss 8-point integr.	
DG P0 CF	discontinuous-Galerkin	displacement	conventional	polynomial order zero, centred flux	
DG P1 CF				polynomial order one, centred flux	
FD D CG 4a	finite-difference	displacement	conventional		4
FD D CG 4b					
FD DS SG 4		displacement-stress	staggered		
SE 4 cn, vn	spectral-element	displacement	conventional	GLL integr.	

Figure 2. Acronyms and essential characteristics of the investigated numerical schemes. Although the FE, DG and SE schemes are constructed on the uniform mesh of cubic elements, we use the term conventional grid also for these schemes because, effectively, all displacement components are located at each node, and stress-tensor components are not explicitly treated. 'order' in the rightmost column means the order of approximation in space.

3.2 The finite-element schemes

Detailed expositions of the FE method can be found, for example, in books by Zienkiewicz & Taylor (1989), Ottosen & Petersson (1992), Hughes (2000), Belytschko *et al*. (2000) and Reddy (2006). For the FE modelling of seismic wave propagation see, for example, Bielak *et al*. (2003), Ma & Liu (2006), Moczo *et al*. (2007a) and Galis *et al*. (2008).

We consider a uniform mesh of cubic elements with eight nodes in vertices and with tri-linear basis functions. Given this, we can get different final FE schemes by considering different volume integrations within an element. The standard full Gauss 8-point integration leads to scheme FE G8. Because the mesh is uniform and medium is homogeneous, the integration is exact. The reduced 8-point Lobatto integration leads to scheme FE L8. Eventually, the application of the simplest possible reduced 1-point Gauss integration leads to scheme FE G1. All the three situations are illustrated in Fig. 1(b).

In the case of the homogeneous medium, uniform FD grids with cubic cells, and mesh of cubic elements, the FE L8 scheme is exactly the same as FD D CG 2, and FE G1 is exactly the same as FD DS PSG 2. Because these are important equalities, we highlight them (for reader's convenience) in the explicit symbolic equations

$$\begin{aligned} \text{FE L8} &= \text{FD D} \quad \text{CG 2} \\ \text{FE G1} &= \text{FD DS PSG 2}. \end{aligned} \tag{7}$$

3.3 The discontinuous-Galerkin scheme

The DG method (e.g. Hesthaven & Warburton 2008) is a discontinuous FE method. Contrary to the classical FE method, no continuity of the basis functions is imposed between elements. Instead, the concept of a numerical flux, taken from the framework of the finite-volume (FV) method (LeVeque 2002) is used for exchanging quantities (e.g. displacements) between elements. Therefore, the DG method supports discontinuities in the seismic wavefield, and provides interesting features for dynamic rupture modelling or wave propagation modelling when high contrasts of the medium properties have to be considered. The DG method has been applied to seismology rather recently (Dumbser &

Käser 2006; Käser & Dumbser 2006; Dumbser *et al*. 2007; Käser *et al*. 2007, 2008; de la Puente *et al*. 2007, 2008; De Basabe *et al*. 2008; de la Puente 2008; Delcourte *et al*. 2009). A wide range of the DG schemes can be obtained depending on the choice of the basis functions (modal or nodal basis functions), the type of flux (upwind or centred flux) or the numerical scheme used for the time integration. Here, we consider a nodal DG scheme with the centred flux (Etienne *et al*. 2010) and we restrict to two of the simplest formulations. The first scheme, DG P0 CF (P0 indicating the zero polynomial of the basis functions, CF centred flux), assumes a uniform representation of wavefields inside the elements (only one constant basis function is used). The second scheme, DG P1 CF, assumes a linear representation of the wavefields inside the elements (via tri-linear basis functions and 8-point Gauss integration). For the homogeneous medium, uniform mesh of cubic elements and the second-order time integration we have the following identities:

$$\begin{aligned}&\text{DG P0 CF} = \text{FV P0 CF} = \text{FE L8} = \text{FD D CG 2}\\ &\text{DG P1 CF} = \text{FE G8}.\end{aligned} \tag{8}$$

Note that in the case of the homogeneous medium, the numerical flux mimics the continuities of quantities and thus leads to direct relation to the classical FE schemes. We may also explicitly emphasize the equivalence of DG P0 CF and FV P0 CF.

3.4 The spectral-element schemes

The power of the SE method to numerically model seismic wave propagation is now well evident from many applications and publications. For details on the method, we refer to the original papers by Komatitsch & Vilotte (1998) and Komatitsch & Tromp (1999) as well as to the comprehensive reviews by Komatitsch *et al*. (2005) and Chaljub *et al*. (2007).

The SE method is a special kind of the FE method that relies on the use of a high-order polynomial basis function. Although in the other investigated schemes, one and the same formula is applied to update a displacement-vector component at all grid positions, in the SE scheme it is necessary to distinguish different schemes for different nodes even in the cubic element. In this paper, we restrict to two representative nodes—the vertex node and the central node. Consequently, we distinguish two schemes—SE 4 cn for the central node and SE 4 vn for the vertex node. The element with the central and vertex nodes is illustrated in Fig. 1(c).

We may also mention the choice of the fourth order. The spectral element calculations in elastodynamics use polynomial orders between 3 and 8. This range of values allows benefiting from the low level of numerical dispersion of the spectral methods (De Basabe & Sen 2007; Seriani & Oliveira 2008) while preventing the use of too severe CFL constraints (due to the quadratic stretching of the grid points near the element edges). The fourth order is, therefore, among the best choices in terms of accuracy and computational costs.

3.5 Unified representation of the numerical schemes

All 13 numerical schemes can be represented in a unified form. Define the V_P/V_S ratio r:

$$r = \alpha/\beta. \tag{9}$$

Throughout the text, r and V_P/V_S, α and V_P, and β and V_S will be used interchangeably. Let h be a grid spacing in each of the three Cartesian directions and Δt be a time step. Let $U_\xi^m = U_\xi^m(I, K, L)$ be a discrete approximation to $u_\xi(Ih, Kh, Lh, m\Delta t) = u_\xi(x_I, y_K, z_L, t_m)$; $\xi \in \{x, y, z\}$. Each numerical scheme can be then written as (compare with eqs (5))

$$\begin{aligned}
U_x^{m+1} &= 2\,U_x^m - U_x^{m-1}\\
&\quad + (\Delta t)^2\,\beta^2\,\{\, r^2\,(D_{xx}[U_x^m] + D_{yx}[U_y^m] + D_{zx}[U_z^m])\\
&\qquad + D_{yy}[U_x^m] - D_{yx}[U_y^m] + D_{zz}[U_x^m] - D_{zx}[U_z^m]\}\\
U_y^{m+1} &= 2\,U_y^m - U_y^{m-1}\\
&\quad + (\Delta t)^2\,\beta^2\,\{\, r^2\,(D_{yy}[U_y^m] + D_{zy}[U_z^m] + D_{xy}[U_x^m])\\
&\qquad + D_{zz}[U_y^m] - D_{zy}[U_z^m] + D_{xx}[U_y^m] - D_{xy}[U_x^m]\}\\
U_z^{m+1} &= 2\,U_z^m - U_z^{m-1}\\
&\quad + (\Delta t)^2\,\beta^2\,\{\, r^2\,(D_{zz}[U_z^m] + D_{xz}[U_x^m] + D_{yz}[U_y^m])\\
&\qquad + D_{xx}[U_z^m] - D_{xz}[U_x^m] + D_{yy}[U_z^m] - D_{yz}[U_y^m]\}\,.
\end{aligned} \tag{10}$$

The numerical schemes differ from each other by the difference operators $D_{\xi\xi}$ and $D_{\xi\eta}$; $\xi, \eta \in \{x, y, z\}$ for approximating second non-mixed and mixed spatial derivatives. Here, we explicitly present D_{xx} and D_{zx} operators. The other operators can be easily obtained by the even permutation of the Cartesian indices.

In the set of the considered 13 numerical schemes, we can recognize two types of non-mixed operators. The first type can be expressed as

$$D_{xx}\,[\Psi(I, K, L)] = \frac{1}{h^2}\sum_{j=0}^{J} w_j^{xx}\,\left[\Psi(I - \Delta_j, K, L) + \Psi(I + \Delta_j, K, L)\right]. \tag{11}$$

Table 1. Grid positions for the D_{xx} operators defined by eq. (11).

D_{xx}^{scheme}	Δ_j				
	$j=0$	$j=1$	$j=2$	$j=3$	$j=4$
$D_{xx}^{\text{FD D CG 2}}$					
$D_{xx}^{\text{FE L8}}$	0	1			
$D_{xx}^{\text{DG P0 CF}}$					
$D_{xx}^{\text{FD DS SG 2}}$	0	1			
$D_{xx}^{\text{FD D CG 4}a}$	0	1	2	3	
$D_{xx}^{\text{FD D CG 4b}}$	0	1	2		
$D_{xx}^{\text{FD DS SG 4}}$	0	1	2	3	
$D_{xx}^{\text{SE 4 cn}}$	0	$\sqrt{12/7}$	2		
$D_{xx}^{\text{SE 4 vn}}$	0	$2-\sqrt{12/7}$	2	$2+\sqrt{12/7}$	4

Table 2. Weight coefficients for the D_{xx} operators defined by eq. (11).

D_{xx}^{scheme}	$576\, w_j^{xx}$				
	$j=0$	$j=1$	$j=2$	$j=3$	$j=4$
$D_{xx}^{\text{FD D CG 2}}$					
$D_{xx}^{\text{FE L8}}$	−576	576			
$D_{xx}^{\text{DG P0 CF}}$					
$D_{xx}^{\text{FD DS SG 2}}$	−576	576			
$D_{xx}^{\text{FD D CG 4}a}$	−400	288	144	−32	
$D_{xx}^{\text{FD D CG 4b}}$	−720	768	−48		
$D_{xx}^{\text{FD DS SG 4}}$	−730	783	−54	1	
$D_{xx}^{\text{SE 4 cn}}$	−480	588	−108		
$D_{xx}^{\text{SE 4 vn}}$	−2520	$294(5+\sqrt{21})$	−384	$294(5-\sqrt{21})$	–36

Here Ψ represents a displacement component. According to eq. (11), operators of different schemes may differ from each other by the number of the grid positions at which displacement components are used for the approximation and the weight coefficients of the considered displacement component at those grid positions. The grid positions and weight coefficients are given in Tables 1 and 2, respectively.

The second type can be expressed as

$$D_{xx}\,[\Psi\,(I,K,L)] = \frac{1}{h^2}\sum_{l=L-1}^{L+1}\sum_{k=K-1}^{K+1}\alpha^{xx}_{l-L+2,\,k-K+2}\;D_{xx}^{\text{FD D CG 2}}\;\Psi\,(I,k,l). \tag{12}$$

The weight coefficients are given in Table 3.

Note that the grid spacing h represents the average spacing between the nodes in the SE schemes. We may emphasize that we consider the exact SEM schemes with no assumption of the regular grid spacing. The average grid spacing h is introduced just to make it possible to directly compare the SE schemes with the other schemes in terms of the spatial sampling ratio. The average grid spacing thus only means how many grid points of the SEM element are used to sample the S wavelength.

Similarly, we can recognize two types of the mixed operators. The first type can be expressed as

$$\begin{aligned} D_{zx}\,[\Psi(I,K,L)] = \frac{1}{h^2}\sum_{n=1}^{N}\sum_{j=1}^{N} w^{zx}_{nj}\,[\;&\Psi(I+\Delta_j,K,L+\Delta_n)-\Psi(I+\Delta_j,K,L-\Delta_n)\\ &-\Psi(I-\Delta_j,K,L+\Delta_n)+\Psi(I-\Delta_j,K,L-\Delta_n)\;]. \end{aligned} \tag{13}$$

The grid positions and weight coefficients are given in Tables 4 and 5, respectively.

The second type can be expressed as

$$D_{zx}\,[\Psi\,(I,K,L)] = \frac{1}{h^2}\sum_{k=K-1}^{K+1}\alpha^{zx}_{k-K+2}\;D_{zx}^{\text{FD D CG 2}}\;\Psi\,(I,k,L). \tag{14}$$

The weight coefficients are given in Table 6.

3.6 Truncation errors of the discrete spatial operators

The truncation error, the difference between the discrete approximation to a derivative and the exact derivative, is an important characteristic of accuracy of the discrete approximation. The lowest power of the argument increment (here, the grid spacing h) determines the order of

Table 3. Weight coefficients for the D_{xx} operators defined by eq. (12).

D_{xx}^{scheme}	α^{xx}
$D_{xx}^{\text{FD DS PSG 2}}$ $D_{xx}^{\text{FE G1}}$	$\frac{1}{16}\begin{bmatrix}1&2&1\\2&4&2\\1&2&1\end{bmatrix}$
$D_{xx}^{\text{FE G8}}$ $D_{xx}^{\text{DG P1 CF}}$	$\frac{1}{36}\begin{bmatrix}1&4&1\\4&16&4\\1&4&1\end{bmatrix}$

Table 4. Grid positions for the D_{zx} operators defined by eq. (13).

D_{zx}^{scheme}	$\Delta_j,\ \Delta_n$			
	$j,n=1$	$j,n=2$	$j,n=3$	$j,n=4$
$D_{zx}^{\text{FD D CG 2}}$				
$D_{zx}^{\text{FE L8}}$	1			
$D_{zx}^{\text{DG P0 CF}}$				
$D_{zx}^{\text{FD DS SG 2}}$	1/2			
$D_{zx}^{\text{FD D CG 4}a}$	1	2		
$D_{zx}^{\text{FD D CG 4b}}$	1	2		
$D_{zx}^{\text{FD DS SG 4}}$	1/2	3/2		
$D_{zx}^{\text{SE 4 cn}}$	$\sqrt{12/7}$	2		
$D_{zx}^{\text{SE 4 vn}}$	$2-\sqrt{12/7}$	2	$2+\sqrt{12/7}$	4

accuracy of the discrete approximation. The coefficients of terms in the truncation error are also important. Table (A1) of the Appendix gives the leading and first higher terms of the truncation errors of all operators defined by eqs (11)–(14). We will discuss the truncation errors in the analysis and interpretation of the numerical results.

4 LOCAL ERROR OF THE NUMERICAL SCHEMES

4.1 Concept of the local error

To evaluate accuracy of the numerical schemes, we define a local error of a numerical scheme. First, we can symbolically express all schemes in a unified form

$$U_{\xi}^{m+1}(I,K,L) = \textit{numerical\_scheme}\ \{U^{m-1},\ U^{m}\}, \tag{15}$$

or, equivalently,

$$U_{\xi}(I,K,L,\ t+\Delta t) = \textit{numerical\_scheme}\ \{U(t-\Delta t),\ U(t)\}. \tag{16}$$

Here, $\xi \in \{x,y,z\}$ and $U(t-\Delta t)$ and $U(t)$ represent displacement components at relevant grid positions around (I,K,L) at times $t-\Delta t$ and t, respectively. Define a numerical solution in one time step as

$$U_{\xi}^{\mathrm{N}}(I,K,L,\ t+\Delta t) = \textit{numerical\_scheme}\ \{U^{\mathrm{E}}(t-\Delta t),\ U^{\mathrm{E}}(t)\}, \tag{17}$$

where the upper index N indicates the numerical solution and the upper index E indicates an exact value. Thus, if we know the exact value of displacement at any time, we can define and calculate a relative local error in amplitude as

$$\varepsilon_{\text{ampl}}^{\text{Rel}} = \left(\frac{\Delta t_{\text{ref}}}{\Delta t}\right)^2 \left|\frac{A^{\mathrm{N}}-A^{\mathrm{E}}}{A^{\mathrm{E}}}\right|. \tag{18}$$

Here, A^{N} is the amplitude of the numerical solution (modulus of the displacement vector) in one time step and A^{E} is the exact amplitude—both evaluated at time $t+\Delta t$. Because different numerical schemes use different time steps Δt, we have to normalize the error for a unit time. Because the time derivative is approximated by the second-order FD formula, we have to normalize with the square of Δt. The division of the relative error by $(\Delta t)^2$, however, artificially increases the value of the error. This can be compensated, for example, by multiplication by some time step value taken as a reference. We specify this later.

In their analysis of the 2-D second-order FD and FE schemes, Moczo *et al*. (2010b) also defined the relative error in the direction of the displacement vector (or error in polarization or angle). The 3-D problem involves three displacement-vector components and two angles. This considerably complicates the quantification of the polarization error and direct comparison of their values with the values of the error

Table 5. Weight coefficients for the D_{zx} operators defined by eq. (13).

D_{zx}^{scheme}	w^{zx}
$D_{zx}^{\text{FD D CG 2}}$	
$D_{zx}^{\text{FE L8}}$	$\frac{1}{4}$
$D_{zx}^{\text{DG P0 CF}}$	
$D_{zx}^{\text{FD DS SG 2}}$	1
$D_{zx}^{\text{FD D CG 4}a}$	$\frac{1}{576}\begin{bmatrix} 256 & -32 \\ -32 & 4 \end{bmatrix}$
$D_{zx}^{\text{FD D CG 4b}}$	$\frac{1}{576}\begin{bmatrix} 240 & -24 \\ -24 & 0 \end{bmatrix}$
$D_{zx}^{\text{FD DS SG 4}}$	$\frac{1}{576}\begin{bmatrix} 729 & -27 \\ -27 & 1 \end{bmatrix}$
$D_{zx}^{\text{SE 4 cn}}$	$\frac{1}{768}\begin{bmatrix} 343 & -21\sqrt{21} \\ -21\sqrt{21} & 27 \end{bmatrix}$
$D_{zx}^{\text{SE 4 vn}}$	$\frac{1}{1152}\begin{bmatrix} 343(5+\sqrt{21}) & -112(7+\sqrt{21}) & 686 & -21(7+\sqrt{21}) \\ -112(7+\sqrt{21}) & 512 & -112(7-\sqrt{21}) & 96 \\ 686 & -112(7-\sqrt{21}) & 343(5-\sqrt{21}) & -21(7-\sqrt{21}) \\ -21(7+\sqrt{21}) & 96 & -21(7-\sqrt{21}) & 18 \end{bmatrix}$

Table 6. Weight coefficients for the D_{zx} operators defined by eq. (14).

D_{zx}^{scheme}	α^{zx}
$D_{zx}^{\text{FD DS PSG 2}}$ $D_{zx}^{\text{FE G1}}$	$\frac{1}{4}\,[\,1 \quad 2 \quad 1\,]$
$D_{zx}^{\text{FE G8}}$ $D_{zx}^{\text{DG P1 CF}}$	$\frac{1}{6}\,[\,1 \quad 4 \quad 1\,]$

in amplitude. Therefore, instead of defining errors analogous to the error used by Moczo *et al*. (2010b), we define the error in the vector difference as

$$\varepsilon_{\text{vdiff}}^{\text{Rel}} = \left(\frac{\Delta t_{ref}}{\Delta t}\right)^2 \frac{1}{A^{\text{E}}}\left[\left(U_x^{\text{N}} - U_x^{\text{E}}\right)^2 + \left(U_y^{\text{N}} - U_y^{\text{E}}\right)^2 + \left(U_z^{\text{N}} - U_z^{\text{E}}\right)^2\right]^{1/2}. \tag{19}$$

This absolute value of the vector difference between the numerically calculated displacement vector and the exact displacement vector comprises both errors in amplitude and polarization in one reasonable value. This value can be directly compared with the error in amplitude.

4.2 Note on the local error and grid dispersion

It is clear that the local error in amplitude, as defined by eq. (18), quantifies, how the exact amplitude changes in one time step due to inaccuracy of a numerical scheme.

In an analysis of stability the problem is different: one investigates condition for propagation of a harmonic plane wave by a numerical scheme in a discrete grid in a stable manner. For example, Moczo *et al*. (2000) investigated condition for propagation of a plane harmonic wave with a constant amplitude by the fourth-order DS staggered grid FD scheme. They obtained the standard stability condition and the grid-dispersion relation. The price for propagating the harmonic plane wave with the constant amplitude in a discrete grid is a grid velocity that differs from the true velocity, and the difference depends on the size of the grid spacing.

4.3 The exact solution–-a harmonic plane *S* wave in an unbounded homogeneous medium

It is reasonable to consider a harmonic plane S wave propagating in an unbounded homogeneous elastic isotropic medium as the exact solution in definitions of the local errors. We will consider a harmonic plane S wave polarized in a vertical plane determined by the z-axis and wavenumber vector $\vec{k}$. The displacement components are

$$u_\xi\,(x, y, z, t\,;\omega\,;\varphi, \delta) = A_\xi E^t E^x E^y E^z\,; \quad \xi \in \{x, y, z\}\,, \tag{20}$$

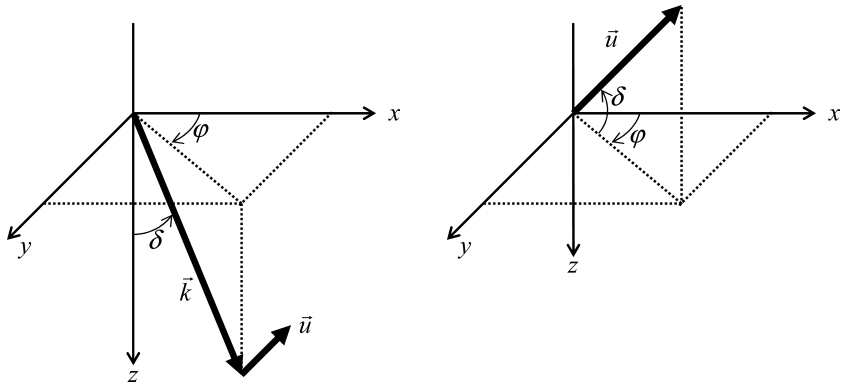

Figure 3. Cartesian coordinate system, angles φ and δ for defining a direction of propagation, displacement vector and displacement components of the plane *S* wave.

where

$$E^t = \exp[-i\omega t]$$

$$E^x = \exp[ik_x x] \qquad E^y = \exp\left[ik_y y\right] \qquad E^z = \exp[ik_z z]$$

$$k_x = k\ \cos\varphi\ \sin\delta \qquad k_y = k\ \sin\varphi\ \sin\delta \qquad k_z = k\ \cos\delta$$

$$A_x = A\ \cos\varphi\ \cos\delta \qquad A_y = A\ \sin\varphi\ \cos\delta \qquad A_z = -A\ \sin\delta$$

$$k = \omega/\beta\ , \quad 0 \le \delta \le \pi\ , \quad 0 \le \varphi \le 2\pi, \tag{21}$$

ω is the angular frequency, $k = |\vec{k}|$ is the wavenumber, δ is the angle between the positive z-axis and the wavenumber vector $\vec{k}$ (the direction of propagation), φ is the angle between the positive x-axis and the vertical plane determined by the z-axis and wavenumber vector $\vec{k}$ (Fig. 3). Note that i in the arguments of the exponential function denotes the imaginary unit throughout the entire text. Otherwise, i will be used to indicate a Cartesian component of the displacement vector or spatial coordinate.

It is known from the numerical experience that modelling of the *P* wave poses a minor problem compared to the modelling of the *S* wave if the modelling comprises both waves. Later, we explain why it is so.

4.4 Evaluation of the exact and numerical values of displacement in a grid

Let h and λ be the grid spacing and wavelength, respectively. The spatial sampling ratio s is defined as

$$s = h/\lambda. \tag{22}$$

Then

$$k = \omega/\beta = 2\pi s/h, \tag{23}$$

$$k_x h = 2\pi s\ \cos\varphi\ \sin\delta\ , \quad k_y h = 2\pi s\ \sin\varphi\ \sin\delta\ , \quad k_z h = 2\pi s\cos\delta, \tag{24}$$

$$\omega = 2\pi s\beta/h. \tag{25}$$

Considering the stability condition for any of the numerical schemes in the form

$$\Delta t \le \Phi(h, \alpha, \beta) \tag{26}$$

and the stability ratio p

$$p = \Delta t\,/\Phi\ , \quad p \le 1, \tag{27}$$

the time step can be expressed as

$$\Delta t = p\ \Phi(h, \alpha, \beta)\,. \tag{28}$$

(Note that the stability parameter sometimes is defined as $p = \Delta t\ \alpha/h$.)

Without loss of generality, consider for simplicity

$$x_I = 0\ , \quad y_K = 0\ , \quad z_L = 0\ , \quad t_m = 0. \tag{29}$$

Then the errors are evaluated at

$$x_I = 0\ , \quad y_K = 0\ , \quad z_L = 0\ , \quad t_{m+1} = \Delta t. \tag{30}$$

The real exact displacement at this space–time grid position is [see eqs (20) and (21)]

$$\mathrm{Re}\left\{u_\xi(0, 0, 0, \Delta t)\right\} = A_\xi \cos\omega\,\Delta t \tag{31}$$

Table 7. Quantities entering the numerical schemes and formulas for the errors.

	$\omega\,\Delta t$	$\Delta t\,\beta/h$	Δt
FD D CG 2 FE L8 DG P0 CF	$2\pi p\,s\,\dfrac{1}{(1+r^2)^{1/2}}$	$\dfrac{p}{(1+r^2)^{1/2}}$	$p\,\dfrac{s}{(1+r^2)^{1/2}}\,\dfrac{\lambda}{\beta}$
FD DS PSG 2 FE G1 FE G8 DG P1 CF	$2\pi p\,s\,\dfrac{1}{r}$	$\dfrac{p}{r}$	$p\,\dfrac{s}{r}\,\dfrac{\lambda}{\beta}$
FD DS SG 2	$2\pi\,\dfrac{1}{\sqrt{3}}\,p\,s\,\dfrac{1}{r}$	$\dfrac{1}{\sqrt{3}}\,p\,\dfrac{1}{r}$	$\dfrac{1}{\sqrt{3}}\,p\,\dfrac{s}{r}\,\dfrac{\lambda}{\beta}$
FD D CG 4a FD D CG 4b	$2\pi 0.7\,p\,s\,\dfrac{1}{(1+r^2)^{1/2}}$	$0.7\,\dfrac{p}{(1+r^2)^{1/2}}$	$0.7p\,\dfrac{s}{(1+r^2)^{1/2}}\,\dfrac{\lambda}{\beta}$
FD DS SG 4	$2\pi\,\dfrac{6}{7\sqrt{3}}\,p\,s\,\dfrac{1}{r}$	$\dfrac{6}{7\sqrt{3}}\,p\,\dfrac{1}{r}$	$\dfrac{6}{7\sqrt{3}}\,p\,\dfrac{s}{r}\,\dfrac{\lambda}{\beta}$
SE 4 cn, vn	$2\pi 0.55\left(\dfrac{1}{2}-\sqrt{\dfrac{3}{28}}\right)p\,s\,\dfrac{1}{r}$	$0.55\left(\dfrac{1}{2}-\sqrt{\dfrac{3}{28}}\right)\dfrac{p}{r}$	$0.55\left(\dfrac{1}{2}-\sqrt{\dfrac{3}{28}}\right)p\,\dfrac{s}{r}\,\dfrac{\lambda}{\beta}$

and

$$A^{\mathrm{E}}=\left[(A_x\cos\omega\,\Delta t)^2+\left(A_y\cos\omega\,\Delta t\right)^2+(A_z\cos\omega\,\Delta t)^2\right]^{1/2}=A\,|\cos\omega\,\Delta t|\,. \tag{32}$$

The exact values of (complex) displacements entering the r.h.s. of schemes (10) are evaluated as

$$\begin{aligned}
&U_\xi^{m-1}(I,K,L)\\
&\quad=u_\xi\,(0,0,0,\ t=-\Delta t\ ;\omega\ ;\varphi,\delta)\\
&\quad=A_\xi\exp[+i\omega\,\Delta t]\\
&U_\xi^{m}(I,K,L)\\
&\quad=u_\xi\,(0,0,0,\ t=0\ ;\omega\ ;\varphi,\delta)\\
&\quad=A_\xi\\
&U_\xi^{m}(I+\Delta_I,K+\Delta_K,L+\Delta_L)\\
&\quad=u_\xi\ (h\,\Delta_I,\ h\,\Delta_K,\ h\,\Delta_L,\ t=0\ ;\omega\ ;\varphi,\delta)\\
&\quad=A_\xi\ \exp[+ik_xh\,\Delta_I]\ \exp[+ik_yh\,\Delta_K]\ \exp[+ik_zh\,\Delta_L]\,.
\end{aligned} \tag{33}$$

The grid-index increments Δ_I, Δ_K and Δ_L depend on a numerical scheme. Quantities k_xh, k_yh and k_zh are given by eq. (24).

It is clear from schemes (10) and definitions of the difference operators (11)–(14) that each scheme effectively includes the second power of quantity $\Delta t\,\beta/h$. Quantities $\omega\,\Delta t$, $\Delta t\,\beta/h$ and Δt entering the numerical schemes and formulae for the errors are summarized in Table 7.

U_x^{m+1}, U_y^{m+1} and U_z^{m+1}, evaluated at (I,K,L), are obtained using schemes (10). Then

$$A^{\mathrm{N}}=\left(\left[\mathrm{Re}\left\{U_x^{m+1}\right\}\right]^2+\left[\mathrm{Re}\left\{U_y^{m+1}\right\}\right]^2+\left[\mathrm{Re}\left\{U_z^{m+1}\right\}\right]^2\right)^{1/2}. \tag{34}$$

In principle, we can take any of the time steps as the reference time step Δt_{ref} appearing in formulae (18) and (19) for the errors. As a reasonable choice we consider

$$\Delta t_{\mathrm{ref}}=\Delta t\quad\text{ for FD DS SG 4 ;}\quad p=0.9,\ \ s=1/6,\ \ r=1.42. \tag{35}$$

The argument for the choice is: as it will be clear from the numerical calculations, scheme FD DS SG 4 is least sensitive to increasing V_P/V_S ratio r, $s=\frac{1}{6}$ is the most common choice for the spatial sampling ratio in the numerical modelling of earthquake motion in surface sedimentary basins using the fourth-order staggered-grid FD scheme, $r=1.42$ is taken in this article instead of the exact minimum value $r=\sqrt{2}$.

Note that the time steps in Table 7 include factor $\frac{s\lambda}{\beta}$. It could be replaced by $\frac{h}{\beta}$ but in both cases the time steps include explicitly the S-wave speed β in addition to the V_P/V_S ratio r. Because, however, the errors (18) and (19) include ratio $(\frac{\Delta t_{\mathrm{ref}}}{\Delta t})^2$ the explicit presence of λ and β is removed from the errors. Consequently, apart from the absolute quantities φ and δ (angles determining the direction of propagation), errors $\varepsilon_{\mathrm{ampl}}^{\mathrm{Rel}}$ and $\varepsilon_{\mathrm{vdiff}}^{\mathrm{Rel}}$ depend only on relative dimensionless quantities—the spatial sampling ratio s, stability ratio p and the V_P/V_S ratio r.

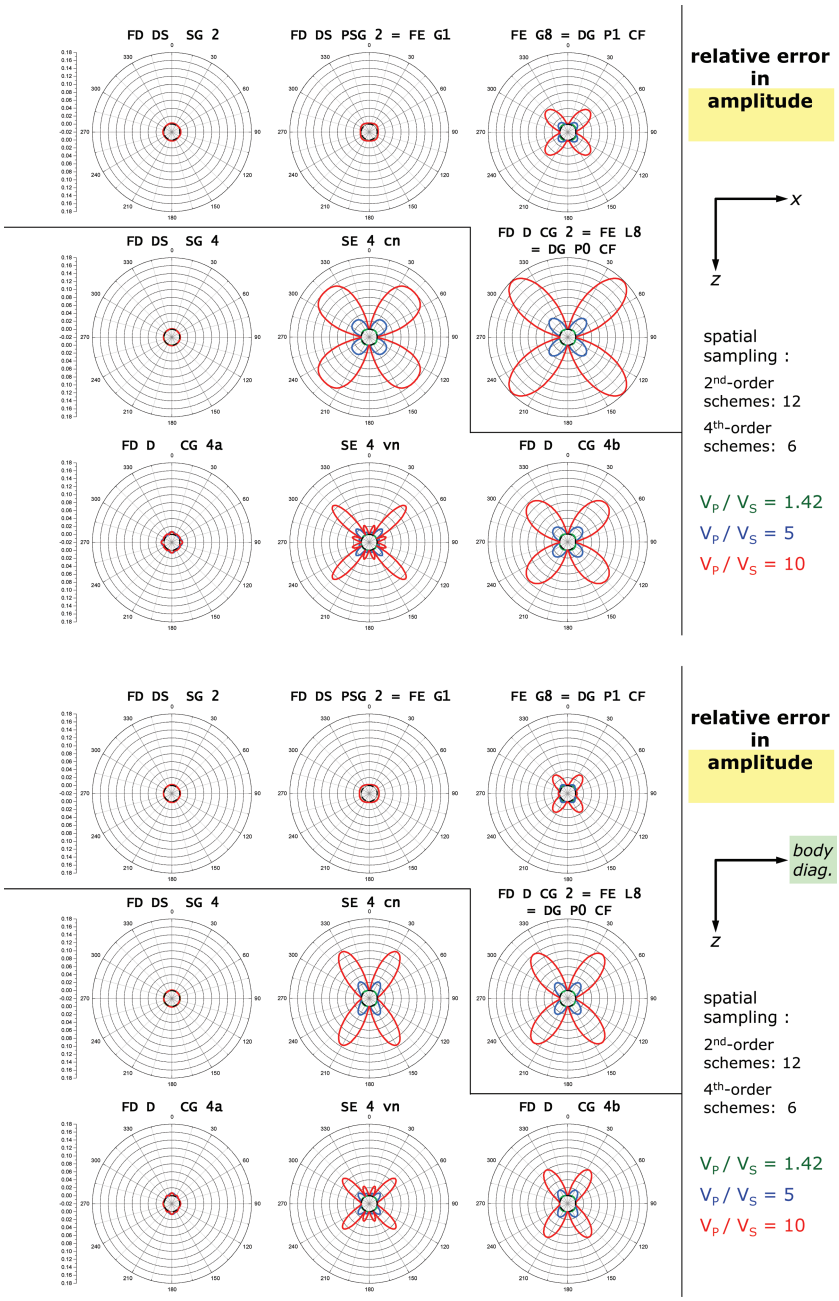

Figure 4. Relative local errors in amplitude for the plane S waves propagating in all directions of the xz-plane (angle $\varphi = 0^\circ$, top panel) and in the vertical plane of the body diagonal (angle $\varphi = 45^\circ$, bottom panel). The errors are calculated for the stability ratio $p = 0.9$, the spatial sampling ratio s corresponding to 12 and 6 grid spacings per wavelength in the second- and fourth-order schemes, respectively, and three values of the V_P/V_S ratio r: 1.42, 5 and 10. In each graph, the innermost circle (black thick solid) of the scale grid corresponds to the zero error.

5 NUMERICAL RESULTS

5.1 Relative local errors in amplitude for plane *S* waves propagating in any direction in the *xz*-plane and vertical plane of the body diagonal

Because the medium is isotropic, it is enough to look at the errors of the schemes for waves propagating in all directions in two planes—for example, the xz-plane and the vertical plane determined by the z-axis and body diagonal.

Fig. 4 shows the relative local errors in amplitude, see definition eq. (18), of all numerical schemes for the plane S waves as functions of direction of propagation in the xz-plane (angle $\varphi = 0^\circ$; top panel) and in the vertical plane of the body diagonal (angle $\varphi = 45^\circ$; bottom panel), that is for all angles δ in both planes. The errors are calculated for the stability ratio $p = 0.9$. The values of the spatial sampling ratio s correspond to 12 and 6 grid spacings per wavelength in the second- and fourth-order schemes, respectively. These spatial samplings are common in the numerical modelling of the earthquake ground motion in sedimentary basins (later, we investigate the error as a function

of s). Recall that in the SE schemes, the grid spacing h represents the average spacing between the nodes to directly compare the SE schemes with the other schemes in terms of the spatial sampling ratio.

The errors were calculated for three values of the V_P/V_S ratio r: 1.42, 5 and 10. The speed ratio $r = 1.42$ represents the minimum possible value of the V_P/V_S ratio r (the exact value being $\sqrt{2}$), $r = 5$ is a common value in surface sediments, mainly under the water level, and $r = 10$, though relatively large, certainly is not the maximum possible value in the unconsolidated surface water-saturated sediments. Practically taken, $r \geq 5$ often have to be accounted for in the numerical modelling of seismic motion in sedimentary basins and valleys.

The thin broken line separates the second- and fourth-order schemes. Within these two parts of the figure, the spatial arrangement of the schemes roughly reflects sensitivity and thus inaccuracy of the schemes with respect to the varying V_P/V_S ratio r. The least sensitive schemes are placed on the left-hand side (l.h.s.).

The figure indicates that the staggered-grid schemes FD DS SG 2 and FD DS SG 4 are both least sensitive and most accurate in the range of the considered V_P/V_S ratio values. Close to them is the partly-staggered-grid scheme FD DS PSG 2 = FE G1. The fourth-order conventional-grid scheme FD D CG 4a comes out as a surprise given the well-known poor behaviour of the most classical conventional-grid scheme FD D CG 2. An immediate notion from comparing FD D CG 4a with FD D CG 4b is that the sensitivity and accuracy with respect to the V_P/V_S ratio r is not dominantly linked to the order of the schemes. An important conclusion also comes from comparison of the three FE schemes. They differ from each other only by the integration within the element but their behaviours with respect to the varying V_P/V_S ratio r differ considerably. The two SE schemes also appear sensitive to the increasing V_P/V_S ratio r and surprisingly inaccurate for V_P/V_S equal to 5 and 10.

5.2 Relative local errors in the vector difference for plane *S* waves propagating in any direction in the *xz*-plane and vertical plane of the body diagonal

The arrangement of Fig. 5 is the same as that of Fig. 4 but Fig. 5 shows the relative errors in the vector difference, see definition eq. (19). The striking difference between Figs 4 and 5 is that for each scheme the error in the vector difference clearly depends on the V_P/V_S ratio r. This difference is the most apparent with the four schemes, FD DS SG 4, FD DS SG 2, FD DS PSG 2 = FE G1 and FD D CG 4a, which were most accurate and least sensitive to the increasing r in terms of the relative error in amplitude. Still, however, the maximum errors of FD DS SG 4 and FD DS SG 2 are smaller than the errors of the other schemes—as in the case of the relative errors in amplitude.

Recall that the relative local error in the vector difference comprises the errors in individual components and, thus, also the error in polarization (difference between the true and numerical directions of the displacement vector). This means that the difference between errors in Fig. 5 and errors in Fig. 4 is due to the polarization errors. Clearly, the polarization errors of each scheme depend on the V_P/V_S ratio r.

5.3 Equivalent spatial sampling for the errors in amplitude and the vector difference

Because the errors shown in Figs 4 and 5 were calculated for the commonly used values of the spatial sampling ratio s, they have only indicative meaning. To quantitatively compare the accuracy of the schemes with respect to varying V_P/V_S ratio r, we proceed as follows. We choose a reference maximum error as the maximum relative error in amplitude of FD DS SG 4 for $r = 10$ and $s = 1/6$. This error is equal to 0.00112. For each individual numerical scheme, we then calculate an equivalent spatial sampling ratio s_{equiv} as a function of r. The equivalent spatial sampling ratio s_{equiv} is defined as a ratio at which the maximum relative error of the scheme is equal to the reference maximum error. The maximum relative error is determined as maximum of errors calculated for angles $\varphi \in [0, 90]^\circ$ and $\delta \in [0, 90]^\circ$ with angle increment of 0.5°. We find the equivalent spatial-sampling ratio based on the relative error in amplitude and the equivalent spatial-sampling ratio based on the relative error in the vector difference.

Fig. 6(a) shows the $1/s_{\text{equiv}}(r)$ curves based on the relative error in amplitude for all the investigated schemes (recall that $1/s_{\text{equiv}}$ is equal to the number of the grid spacings per wavelength). The left-hand panel shows the curves for the stability ratio $p = 0.3$, the right-hand panel for $p = 0.9$. The solid lines are used for the fourth-order schemes, the dashed lines for the second-order schemes.

The curves for the two values of the stability ratio differ from each other only negligibly. Small differences can be seen only for the lowest values of r.

At first sight, we realize that the curves are consistent with the indicative Fig. 4. FD DS SG 4, FD D CG 4a, FD DS SG 2 and FD DS PSG 2 = FE G1 make one distinct group of schemes. The equivalent sampling ratios of these schemes only little depend on the V_P/V_S ratio r.

FD D CG 4b, SE 4 cn, SE 4 vn, FE G8 = DG P1 CF and FD D CG 2 = FE L8 = DG P0 CF make the other distinct group of schemes whose equivalent spatial sampling ratios considerably change with increasing V_P/V_S ratio r. Among the schemes of the second group, we can distinguish the subgroup of the FD D CG 4b, SE 4 cn and SE 4 vn schemes, distinct FE G8 = DG P1 CF, and, finally, the worst FD D CG 2 = FE L8 = DG P0 CF.

Fig. 6(b) shows the $1/s_{\text{equiv}}(r)$ curves based on the relative error in the vector difference. As indicated by Fig. 5 the $1/s_{\text{equiv}}$ increase with increasing r for each scheme.

Fig. 6 clearly shows that, in terms of the equivalent spatial sampling, FD DS SG 4 is more accurate and more efficient than the other schemes for media with $r > 2$.

Table 8 lists the $1/s_{\text{equiv}}$ values for $p = 0.9$ and three values of the V_P/V_S ratio r—1.42, 5 and 10.

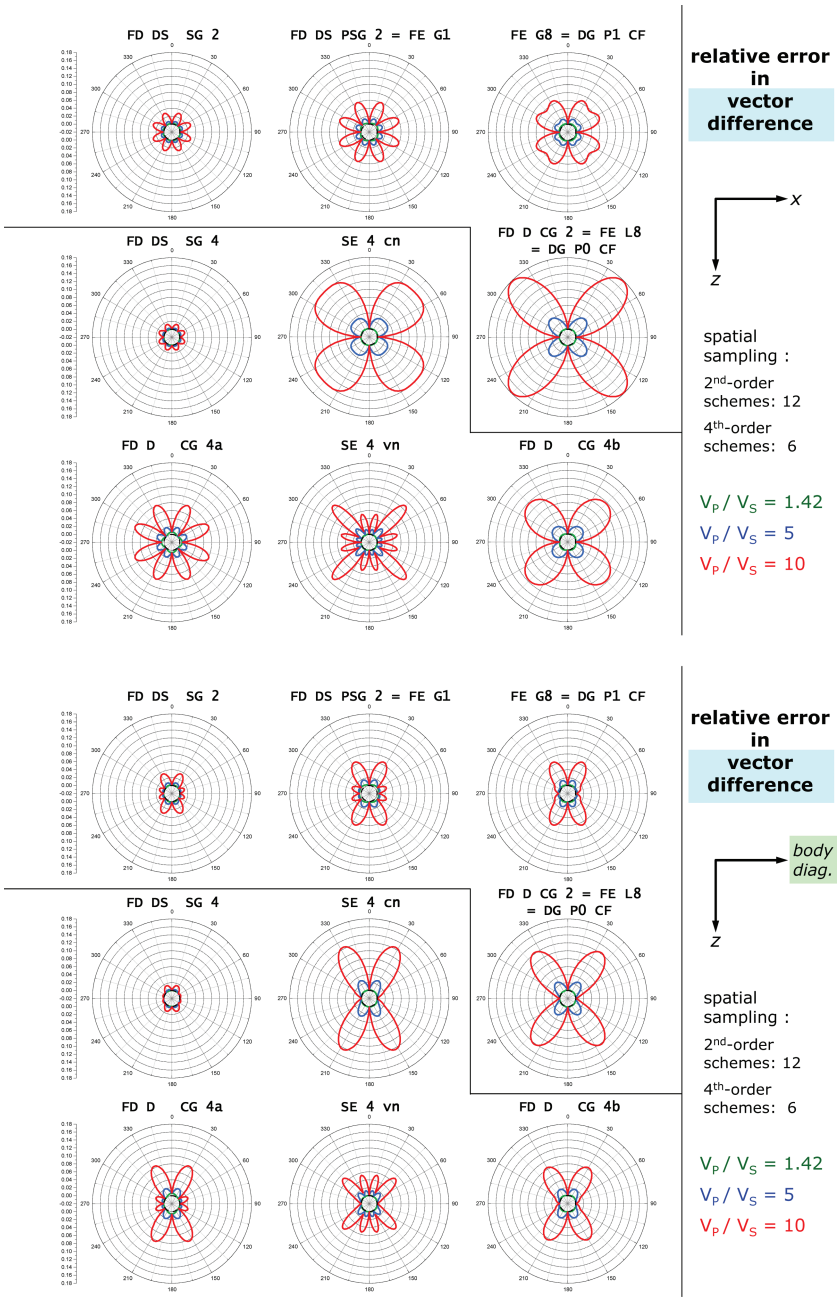

Figure 5. The same as Fig. 4 but for the errors in the vector difference.

5.4 Essential summary of the numerical results

The relative local error in amplitude of schemes FD DS SG 4, FD D CG 4a, FD DS SG 2 and FD DS PSG 2 = FE G1 is almost independent on the V_P/V_S ratio r. However, the error in the vector difference increases with increasing V_P/V_S ratio. This can be explained only by the dependence of the polarization errors of all schemes on the V_P/V_S ratio. The dependence of the error in the vector difference on the V_P/V_S ratio has to be accounted for by a proper spatial sampling.

FD D CG 2 = FE L8 = DG P0 CF is the most sensitive to increasing V_P/V_S ratio and for $V_P/V_S > 2$ requires considerably denser spatial sampling than any other scheme.

The maximum errors in the vector difference of schemes FD DS SG 2, FE G8 = DG P1 CF and FD DS PSG 2 = FE G1 increase with the increasing V_P/V_S ratio in the same way. Schemes FD DS PSG 2 = FE G1 and FE G8 = DG P1 CF require denser spatial sampling than FD DS SG 2 to achieve the same accuracy.

The maximum errors in the vector difference of all fourth-order schemes increase for $V_P/V_S > 3$ in the same way. Schemes FD D CG 4a, FD D CG 4b, SE 4 cn and SE 4 vn require denser spatial sampling than FD DS SG 4 to achieve the same accuracy.

The fourth-order schemes are for $V_P/V_S > 3$ less sensitive to increasing V_P/V_S ratio than the second-order schemes.

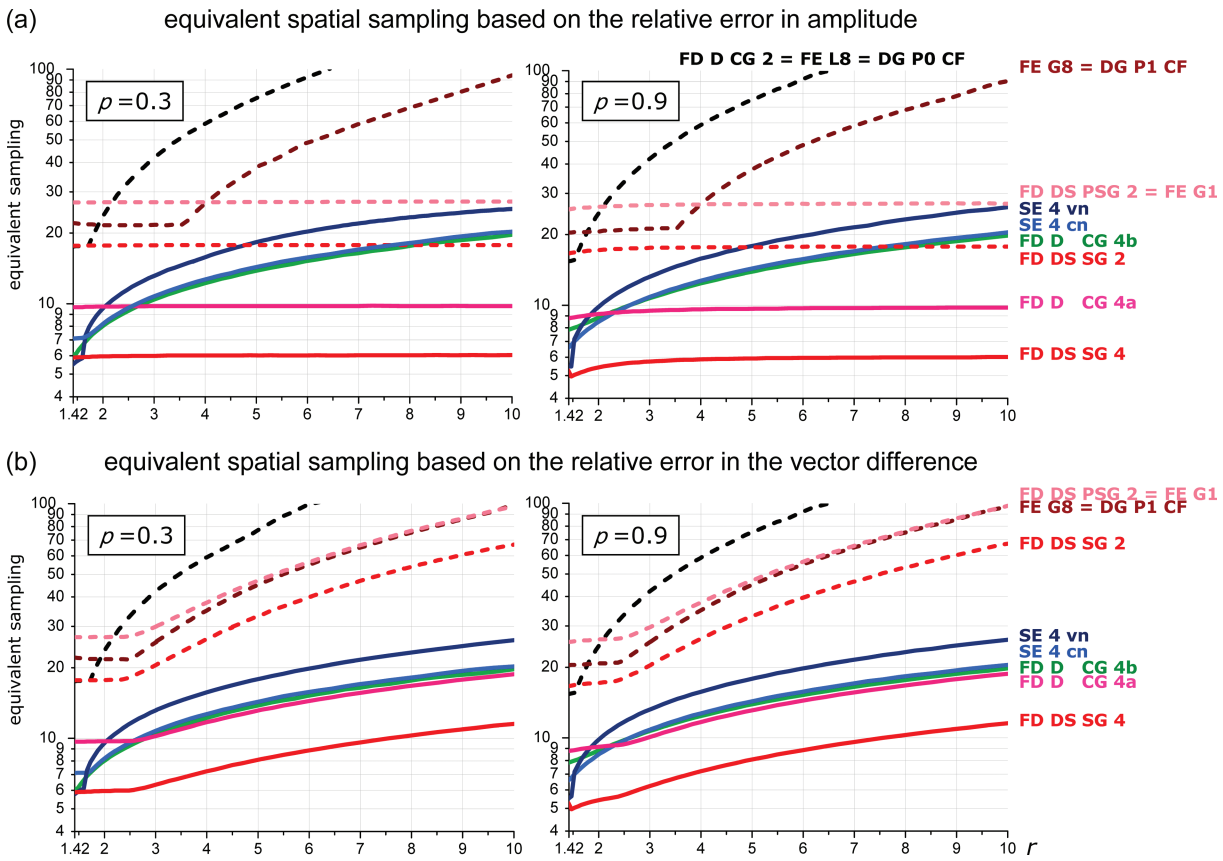

Figure 6. The $1/s_{\text{equiv}}(r)$ curves. The equivalent spatial sampling ratio s_{equiv} is defined as a ratio at which the maximum absolute value of the relative error of the scheme is equal to the reference maximum error. The chosen reference maximum error, 0.00112, is equal to the maximum relative error in amplitude of FD DS SG 4 for the V_P/V_S ratio $r = 10$ and spatial sampling ratio $s = 1/6$. The left-hand panel shows the curves for the stability ratio $p = 0.3$, the right-hand panel for $p = 0.9$.

Table 8. The $1/s_{\text{equiv}}$ values for the stability ratio $p = 0.9$ and reference maximum error equal to 0.00112. Boldface indicates schemes for which the $1/s_{\text{equiv}}$ based on the relative error in amplitude varies with the V_P/V_S ratio r only negligibly.

V_P/V_S ratio r	**FD DS SG 4**	**FD D CG 4a**	**FD DS SG 2**	FD D CG 4b	SE 4 cn	**FD DS PSG 2 = FE G1**	SE 4 vn	FE G8 = DG P1 CF	FD D CG 2 = FE L8 = DG P0 CF
				$1/s_{\text{equiv}}$ based on the relative error in amplitude					
1.42	**5.3**	**8.8**	**16.6**	7.8	6.6	**25.6**	5.5	17.7	15.4
5	**5.9**	**9.7**	**17.7**	14.0	14.4	**26.9**	18.0	38.7	75.4
10	**6.0**	**9.7**	**17.8**	19.7	20.4	**27.1**	26.2	85.3	153.5
				$1/s_{\text{equiv}}$ based on the relative error in the vector difference					
1.42	**5.3**	**8.8**	**16.6**	7.8	6.6	**25.6**	5.5	20.4	15.4
5	**8.1**	**13.1**	**33.3**	14.0	14.4	**47.5**	18.0	45.6	76.3
10	**11.5**	**18.7**	**67.3**	19.8	20.5	**97.5**	26.2	97.0	162.1

6 ANALYSIS AND INTERPRETATION OF THE NUMERICAL RESULTS

6.1 How does the equation of motion see the *S* and *P* waves?

Recall the equation of motion (5) in the concise form

$$u_{i,tt} = \alpha^2 u_{j,ji} + \beta^2 (u_{i,jj} - u_{j,ji}). \tag{36}$$

The *S* wave is solenoidal, that is, div $\vec{u} = u_{j,j} = 0$. Consequently, in the case of the *S* wave, we have

$$u_{j,ji} = 0, \quad u_{i,jj} - u_{j,ji} = \frac{1}{\beta^2} u_{i,tt}. \tag{37}$$

The P wave is irrotational, that is, $\mathrm{rot}\,\vec{u} = 0$ or $\varepsilon_{kji}\,u_{i,j} = 0$, where ε_{kji} is the Levi-Civita symbol. Consequently, in the case of the P wave it is

$$u_{j,ji} = \frac{1}{\alpha^2} u_{i,tt} \quad , \quad u_{i,jj} - u_{j,ji} = 0. \tag{38}$$

6.2 How does a numerical scheme see the *S* and *P* waves?

A numerical scheme solving equation of motion (36) can be written in the form

$$DA\{u_{i,tt}\} \approx \alpha^2 DA\{u_{j,ji}\} + \beta^2 DA\{\, u_{i,jj} - u_{j,ji}\,\}, \tag{39}$$

where DA means a discrete approximation. Eq. (39) is, in fact, a concise symbolic form of eqs (10). A discrete approximation to any operator in general can be expressed as a sum of the exact differential operator and a truncation error (for which we will use symbol TrE). Eq. (39) can be written as

$$u_{i,tt} + TrE\{u_{i,tt}\} \approx \alpha^2(\, u_{j,ji} + TrE\{u_{j,ji}\}\,) + \beta^2(\, u_{i,jj} - u_{j,ji} + TrE\{\, u_{i,jj} - u_{j,ji}\,\}\,). \tag{40}$$

6.2.1 The case of the harmonic plane S wave

Considering the first of eqs (37), equality $u^S_{i,tt} = -\omega^2 u^S_i$, and the fact that each second spatial derivative of a displacement-vector component is proportional to $-\omega^2 u^S_i/\beta^2$, eq. (40) can be rewritten as

$$\left(1 + error_i^{t\,S}\right)\left(-\omega^2 u_i^S\right) \approx \alpha^2\left(0 + error_i^{\alpha S}\right)\frac{-\omega^2 u_i^S}{\beta^2} + \beta^2\left(1 + error_i^{\beta S}\right)\frac{-\omega^2 u_i^S}{\beta^2} \tag{41}$$

and

$$u_i^S \approx \left(r^2\, error_i^{\alpha S} + 1 + error_i^{\beta S} - error_i^{t\,S}\right)\; u_i^S. \tag{42}$$

Note that the double-index summation rule does not apply to index i from eqs (41)–(57).

The error terms

$$error_i^{\alpha S} = \frac{\beta^2\; TrE\left\{\, u^S_{j,ji}\,\right\}}{-\omega^2\, u_i^S}\;, \quad error_i^{\beta S} = \frac{\beta^2\; TrE\left\{\, u^S_{i,jj} - u^S_{j,ji}\,\right\}}{-\omega^2\, u_i^S} \tag{43}$$

do not depend on r. The error term $error_i^{t\,S}$ does depend on r

$$error_i^{t\,S} = \frac{TrE\left\{u^S_{i,tt}\right\}}{-\omega^2\, u_i^S} = c_1\frac{1}{r^2} + c_2\frac{1}{r^4} + \cdots \tag{44}$$

Coefficients c_l ; $l = 1, 2, \ldots$ do not depend on r. Note that the series in powers of $\frac{1}{r^2}$ is due to the second-order approximation to the second time derivative. The squares of the time step, $(\Delta t)^2$, are expressed using $\frac{1}{r^2}$.

6.2.2 The case of the harmonic plane P wave

Considering the second of eqs (38), equality $u^P_{i,tt} = -\omega^2 u^P_i$, and the fact that each second spatial derivative of a displacement-vector component is proportional to $-\omega^2 u^P_i/\alpha^2$, eq. (40) can be rewritten as

$$\left(1 + error_i^{t\,P}\right)\left(-\omega^2 u_i^P\right) \approx \alpha^2\left(1 + error_i^{\alpha P}\right)\frac{-\omega^2 u_i^P}{\alpha^2} + \beta^2\left(0 + error_i^{\beta P}\right)\frac{-\omega^2 u_i^P}{\alpha^2} \tag{45}$$

and

$$u_i^P \approx \left(1 + error_i^{\alpha P} + \frac{1}{r^2}\, error_i^{\beta P} - error_i^{t\,P}\right)\; u_i^P. \tag{46}$$

Analogously to the error terms in eqs (43), $error_i^{\alpha P}$ and $error_i^{\beta P}$ do not depend on r. The dependence of $error_i^{t\,P}$ on r is analogous to that of $error_i^{t\,S}$ in eq. (44).

6.2.3 Comparison

We see the important difference between eq. (42) for the S wave and eq. (46) for the P wave: In the case of the S wave, term $r^2 error_i^{\alpha S}$ increases with increasing V_P/V_S ratio r, whereas in the case of the P wave, term $\frac{1}{r^2} error_i^{\beta P}$ decreases with increasing V_P/V_S ratio r. This is why a large value of the V_P/V_S ratio r does not pose a problem for the P wave.

Because we restrict our investigation to the S wave, in the following section, we will omit the explicit indication of the S wave in the displacement-vector components and error terms.

6.3 Structure of the relative errors in amplitude and vector difference

Recall eq. (39)

$$DA\{u_{i,tt}\} \approx \alpha^2 DA\{u_{j,ji}\} + \beta^2 DA\{u_{i,jj} - u_{j,ji}\}. \tag{47}$$

The investigated numerical schemes differ from each other by the approximations on the r.h.s. They share the same approximation to the second time derivative

$$DA\{u_{i,tt}\} \approx \left(u_i^{m+1} - 2u_i^m + u_i^{m-1}\right) \frac{1}{(\Delta t)^2}. \tag{48}$$

After substituting $DA\{u_{i,tt}\}$ in eq. (47) by approximation (48), we can get the scheme for the numerical displacement component at the time level $m+1$ in the form

$${}^{\mathrm{N}}u_i^{m+1} = 2u_i^m - u_i^{m-1} + (\Delta t)^2 \left(\alpha^2 DA\{u_{j,ji}\} + \beta^2 DA\{u_{i,jj} - u_{j,ji}\}\right). \tag{49}$$

Recalling the concept of the local error, eqs (15)–(19), we distinguish the numerical value, labelled N, on the l.h.s., from the exact values of the displacement components on the r.h.s. (not labelled). Subtracting u_i^{m+1} from both sides of eq. (49), dividing the equation by $(\Delta t)^2$ and using eq. (48), we get

$$\left({}^{\mathrm{N}}u_i^{m+1} - u_i^{m+1}\right) \frac{1}{(\Delta t)^2} = -DA\{u_{i,tt}\} + \alpha^2 DA\{u_{j,ji}\} + \beta^2 DA\{u_{i,jj} - u_{j,ji}\}. \tag{50}$$

Each of the discrete approximations on the r.h.s. can be replaced by the sum of the exact operator and truncation error. Then

$$\begin{aligned}\left({}^{\mathrm{N}}u_i^{m+1} - u_i^{m+1}\right) \frac{1}{(\Delta t)^2} &= -u_{i,tt} + \alpha^2 u_{j,ji} + \beta^2 (u_{i,jj} - u_{j,ji}) \\ &\quad - TrE\{u_{i,tt}\} + \alpha^2 TrE\{u_{j,ji}\} + \beta^2 TrE\{u_{i,jj} - u_{j,ji}\}.\end{aligned} \tag{51}$$

The sum of the first three terms on the r.h.s. is equal to zero, see eq. (36), and thus

$$\left({}^{\mathrm{N}}u_i^{m+1} - u_i^{m+1}\right) \frac{1}{(\Delta t)^2} = -TrE\{u_{i,tt}\} + \alpha^2 TrE\{u_{j,ji}\} + \beta^2 TrE\{u_{i,jj} - u_{j,ji}\}. \tag{52}$$

Considering eqs (43) and (44), the case of the harmonic plane S wave,

$$\left({}^{\mathrm{N}}u_i^{m+1} - u_i^{m+1}\right) \frac{1}{(\Delta t)^2} = \left(error_i^{t\,S} - r^2 error_i^{\alpha S} - error_i^{\beta S}\right) \omega^2 u_i. \tag{53}$$

Referring to definition (19) of the error in the vector difference and eq. (32), we can consider an auxiliary error-component term

$$\begin{aligned}\tilde{\varepsilon}_{i,\,\mathrm{vdiff}} &= \frac{\left({}^{\mathrm{N}}u_i^{m+1} - u_i^{m+1}\right)}{A^{\mathrm{E}}} \frac{1}{(\Delta t)^2} \\ &= \left(error_i^{t\,S} - r^2 error_i^{\alpha S} - error_i^{\beta S}\right) \frac{\omega^2 u_i}{|A \cos \omega\, \Delta t|}.\end{aligned} \tag{54}$$

Referring now to definition (18) of the error in amplitude and eq. (32), we can rearrange eq. (54) and consider an auxiliary error-component term

$$\begin{aligned}\tilde{\varepsilon}_{i,\,\mathrm{ampl}} &= \frac{{}^{\mathrm{N}}u_i^{m+1}}{A^{\mathrm{E}}} \frac{1}{(\Delta t)^2} \\ &= \left(error_i^{t\,S} - r^2 error_i^{\alpha S} - error_i^{\beta S}\right) \frac{\omega^2 u_i}{|A \cos \omega\, \Delta t|} + \frac{u_i^{m+1}}{|A \cos \omega\, \Delta t|} \frac{1}{(\Delta t)^2}.\end{aligned} \tag{55}$$

Accounting for eqs (20) and (21), we have

$$u_i^{m+1} = u_i(t + \Delta t) = \exp[-i\,\omega\,\Delta t]\;\; u_i(t). \tag{56}$$

Consequently,

$$\begin{aligned}\tilde{\varepsilon}_{i\,,\,\mathrm{ampl}} &= \frac{{}^{\mathrm{N}}u_i^{m+1}}{A^{\mathrm{E}}} \frac{1}{(\Delta t)^2} \\ &= \left(error_i^{t\,S} - r^2 error_i^{\alpha S} - error_i^{\beta S} + \frac{\exp[-i\,\omega\,\Delta t]}{(\omega\,\Delta t)^2}\right) \frac{\omega^2 u_i}{|A \cos \omega\, \Delta t|}.\end{aligned} \tag{57}$$

The errors in the vector difference (19) and amplitude (18) can be then written as

$$\varepsilon_{\mathrm{vdiff}}^{\mathrm{Rel}} = (\Delta t_{\mathrm{ref}})^2 \left[\tilde{\varepsilon}_{x,\,\mathrm{vdiff}}^2 + \tilde{\varepsilon}_{y,\,\mathrm{vdiff}}^2 + \tilde{\varepsilon}_{z,\,\mathrm{vdiff}}^2\right]^{1/2} \tag{58}$$

and

$$\varepsilon_{\mathrm{ampl}}^{\mathrm{Rel}} = (\Delta t_{\mathrm{ref}})^2 \left| \left[\tilde{\varepsilon}_{x,\,\mathrm{ampl}}^2 + \tilde{\varepsilon}_{y,\,\mathrm{ampl}}^2 + \tilde{\varepsilon}_{z,\,\mathrm{ampl}}^2\right]^{1/2} - 1 \right|. \tag{59}$$

Although the auxiliary error-component terms eqs (54) and (57) do not quantitatively represent the entire values of the relative errors in amplitude and the vector difference, they indicate where the difference between the error in amplitude and error in the vector difference comes from. The r.h.s of eqs (54) and (57) differ by the fourth term in the parenthesis in eq. (57). The absolute value of this term is proportional to r^2, see Table 7. The fact that the errors in amplitude of schemes FD DS SG 4, FD D CG 4a, FD DS SG 2 and FD DS PSG 2 = FE G1 are almost independent on r is likely related to the interaction of the second and fourth terms, as they are both proportional to r^2.

6.4 Truncation errors of the discrete approximations to the second non-mixed and mixed spatial derivatives

It is also reasonable to look at the truncation errors of the discrete approximations to the second non-mixed and mixed spatial derivatives. The leading and first higher terms of the truncation errors of the second- and fourth-order operators are listed in Table A1 in Appendix. Here, we compare coefficients of these terms.

Denote the truncation errors of the operators for the mixed and non-mixed derivatives as $TrE\{D_{zx}\}$ and $TrE\{D_{xx}\}$, respectively. Define ratios for each scheme

$$C_{LT} = \frac{\text{coeff. of the leading term of } TrE\{Dzx\}}{\text{coeff. of the leading term of } TrE\{Dxx\}}$$
$$C_{kHT} = \frac{\text{coeff. of the k-th higher term of } TrE\{Dzx\}}{\text{coeff. of the k-th higher term of } TrE\{Dxx\}}; \quad k = 1, 2, 3, \ldots \tag{60}$$

C_{LT} and C_{1HT} are shown in Fig. 7. Fig. 7(a) includes the four schemes for which the errors in amplitude are almost independent on the V_P/V_S ratio r, Fig. 7(b) includes all other schemes. All the four schemes in Fig. 7(a) have $C_{LT} = 1$. It is easy to find that schemes FD DS SG 4, FD DS SG 2 and FD DS PSG 2 = FE G1 have also $C_{kHT} = 1$. On the other hand, none of schemes in Fig. 7(b) has C_{LT} or C_{1HT} equal to 1.

Let c_2^2 and c_4^2 be coefficients of the leading term and first higher term of $TrE\{D_{xx}\}$ or $TrE\{D_{zx}\}$ of the second-order FD DS SG 2 operators. The upper index indicates the second-order, the lower index the power of the grid spacing h. Similarly, let c_4^4 and c_6^4 be coefficients of the leading term and first higher term of $TrE\{D_{xx}\}$ or $TrE\{D_{zx}\}$ of the fourth-order FD DS SG 4 operators. Fig. 7 shows the corresponding coefficients of other second-order operators as multiples of c_2^2 and c_4^2. Similarly, the figure also shows coefficients of other fourth-order operators as multiples of c_4^4 and c_6^4.

In general, for the schemes of the same order (that is either second or fourth) for given C_{LT} or C_{1HT} the errors in amplitude and the vector difference increase with increasing absolute values of coefficients of terms in the truncation errors. This can be well seen in the case of schemes FD DS SG 2 and FD DS PSG 2 = FE G1 and schemes SE 4 cn and SE 4 vn. In both comparisons, the C_{LT} or C_{1HT} ratios are the same for the compared schemes but the coefficients of terms in the truncation errors are different.

It is interesting to compare FD DS SG 4 and FD D CG 4a. Although they have different C_{1HT}, the ratio of the coefficients of the leading terms (7.1, see Fig. 7a) well quantifies the difference in their errors (see Fig. 6).

7 CONCLUSIONS

We considered an unbounded homogeneous isotropic elastic medium and uniform cubic grid, and analysed 13 3-D time-domain explicit numerical schemes of the second-order in time for modelling seismic wave propagation and earthquake motion for their behaviour with a varying P-wave to S-wave speed ratio (V_P/V_S or r).

The schemes of the second-order in space are:

FD D CG 2—finite-difference displacement conventional grid
FD DS PSG 2—finite-difference displacement-stress partly-staggered grid
FD DS SG 2—finite-difference displacement-stress staggered grid
FE L8—finite-element Lobatto 8-integration points
FE G1—finite-element Gauss 1-integration point
FE G8—finite-element Gauss 8-integration points
DG P0 CF—discontinuous-Galerkin polynomial order zero centred-flux
DG P1 CF—discontinuous-Galerkin polynomial order one centred -flux

The schemes of the fourth-order in space are:

FD D CG 4a—finite-difference displacement conventional grid variant a
FD D CG 4b—finite-difference displacement conventional grid variant b
FD DS SG 4—finite-difference displacement-stress staggered grid
SE 4 cn—spectral-element central node
SE 4 vn—spectral-element vertex node.

We wrote all schemes in the unified form. Some of the schemes are equivalent

FD D CG 2 = FE L8 = DG P0 CF
FD DS PSG 2 = FE G1
FE G8 = DG P1 CF.

We defined the numerical solution as the displacement vector at time level $m + 1$ obtained from the numerical scheme entered by the exact values of displacement of the plane S wave at time levels $m - 1$ and m. We defined the relative local error in amplitude and the relative local error in the vector difference based on the difference between the numerical solution and the exact solution. Because different schemes use different time steps, we normalized the errors for a unit time.

(a)

2nd-order schemes			4th-order schemes		
operator	C_{LT} C_{1HT}		operator	C_{LT} C_{1HT}	
$D_{xx}^{\text{FD DS SG 2}}$	1 1	c_2^2 c_4^2	$D_{xx}^{\text{FD DS SG 4}}$	1 1	c_4^4 c_6^4
$D_{zx}^{\text{FD DS SG 2}}$		c_2^2 c_4^2	$D_{zx}^{\text{FD DS SG 4}}$		c_4^4 c_6^4
$D_{xx}^{\text{FD DS PSG 2}}$ $D_{xx}^{\text{FE G1}}$	1 1	$7.0\ c_2^2$ $53.5\ c_4^2$	$D_{xx}^{\text{FD D CG 4}a}$	1 0.53	$7.1\ c_4^4$ $26.7\ c_6^4$
$D_{zx}^{\text{FD DS PSG 2}}$ $D_{zx}^{\text{FE G1}}$		$7.0\ c_2^2$ $53.5\ c_4^2$	$D_{zx}^{\text{FD D CG 4}a}$		$7.1\ c_4^4$ $14.2\ c_6^4$

(b)

2nd-order schemes			4th-order schemes		
operator	C_{LT} C_{1HT}		operator	C_{LT} C_{1HT}	
$D_{xx}^{\text{FE G8}}$ $D_{xx}^{\text{DG P1 CF}}$	1.2 1.73	$5.0\ c_2^2$ $31.0\ c_4^2$	$D_{xx}^{\text{FD D CG 4b}}$	8.5 22	$1.2\ c_4^4$ $1.8\ c_6^4$
$D_{zx}^{\text{FE G8}}$ $D_{zx}^{\text{DG P1 CF}}$		$6.0\ c_2^2$ $53.5\ c_4^2$	$D_{zx}^{\text{FD D CG 4b}}$		$10.1\ c_4^4$ $39.1\ c_6^4$
$D_{xx}^{\text{FD D CG 2}}$ $D_{xx}^{\text{FE L8}}$ $D_{xx}^{\text{DG P0 CF}}$	4 16	c_2^2 c_4^2	$D_{xx}^{\text{SE 4 cn}}$	6 8	$2.03\ c_4^4$ $3.5\ c_6^4$
$D_{zx}^{\text{FD D CG 2}}$ $D_{zx}^{\text{FE L8}}$ $D_{zx}^{\text{DG P0 CF}}$		$4.0\ c_2^2$ $16.0\ c_4^2$	$D_{zx}^{\text{SE 4 cn}}$		$12.2\ c_4^4$ $27.9\ c_6^4$
			$D_{xx}^{\text{SE 4 vn}}$	6 8	$5.4\ c_4^4$ $106.8\ c_6^4$
			$D_{zx}^{\text{SE 4 vn}}$		$32.5\ c_4^4$ $854.5\ c_6^4$

Figure 7. Comparison of coefficients of the leading and the first higher terms of the truncation errors $TrE\{D_{xx}\}$ and $TrE\{D_{zx}\}$. (a) schemes with the error in amplitude almost independent on the V_P/V_S ratio r. (b) schemes with the error in amplitude dependent on the V_P/V_S ratio r.

We also defined the equivalent spatial sampling ratio as a ratio at which the maximum relative error of the scheme is equal to the reference maximum error.

The numerical evaluations of the errors and equivalent spatial sampling ratios led to the following conclusions:

The relative local error in amplitude of schemes FD DS SG 4, FD D CG 4a, FD DS SG 2 and FD DS PSG 2 = FE G1 is almost independent on the V_P/V_S ratio. The error in the vector difference increases with increasing V_P/V_S ratio. This can be explained only by the dependence of the polarization errors of all schemes on the V_P/V_S ratio.

FD D CG 2 = FE L8 = DG P0 CF is the most sensitive to the increasing V_P/V_S ratio and for $V_P/V_S > 2$ requires considerably denser spatial sampling than any other scheme.

The maximum errors in the vector difference of the second-order schemes FD DS SG 2, FE G8 = DG P1 CF and FD DS PSG 2 = FE G1 increase with the increasing V_P/V_S ratio in the same way. Schemes FD DS PSG 2 = FE G1 and FE G8 = DG P1 CF require denser spatial sampling than FD DS SG 2 to achieve the same accuracy.

The maximum errors in the vector difference of all the fourth-order schemes increase with the increasing V_P/V_S ratio for $V_P/V_S > 3$ in the same way. Schemes FD D CG 4a, FD D CG 4b, SE 4 cn and SE 4 vn require denser spatial sampling than FD DS SG 4 to achieve the same accuracy.

The fourth-order schemes are for $V_P/V_S > 3$ less sensitive to the increasing V_P/V_S ratio than the second-order schemes.

We theoretically showed how a numerical scheme sees the P wave and S wave if the V_P/V_S ratio increases. In this study, we show that the increasing V_P/V_S ratio does not pose a problem for a scheme to model the P wave.

We also showed the structure of the errors in amplitude and the vector difference.

We compared the schemes in terms of the truncation errors of the discrete approximations to the second mixed and non-mixed spatial derivatives. The most important finding is this: Schemes FD DS SG 4, FD D CG 4a, FD DS SG 2 and FD DS PSG 2 = FE G1 with the errors in amplitude almost independent on the V_P/V_S ratio have the same coefficients of the leading terms of the truncation errors of approximations to the second mixed and non-mixed spatial derivatives. None of the other schemes have those coefficients equal.

Scheme FD DS SG 2 with the smallest errors among the second-order schemes and scheme FD DS SG 4 with the smallest errors among the fourth-order schemes have the same coefficients also at each higher term of the truncation errors of approximations to the second mixed and non-mixed spatial derivatives. The absolute values of the coefficients are smaller than the absolute values of coefficients of the truncation errors of the other schemes.

The general theoretical conclusion based on the investigation of the 13 numerical schemes is that the homogeneity of the approximations to the second mixed and non-mixed spatial derivatives in terms of the coefficients of the leading terms of their truncation errors as well as the absolute values of the coefficients are key factors for the behaviour of the numerical schemes with increasing V_P/V_S ratio.

The practical conclusion for the existing numerical schemes is that the dependence of the errors in the vector difference on the V_P/V_S ratio should be accounted for by a proper (sufficiently dense) spatial sampling. We quantified the proper sampling with respect to the local errors in amplitude and in the vector difference.

ACKNOWLEDGMENTS

This work was supported in part by the Slovak Research and Development Agency under the contract number APVV-0435-07 (project OPTIMODE) and bilateral APVV Slovak–French project SK-FR-0028-09. We gratefully acknowledge the funding by the European Union through the Initial Training Network QUEST (Grant agreement number 238007), a Marie Curie Action under the People Programme. We thank Jean Virieux and Jacobo Bielak for discussions. We very much appreciate careful and useful reviews by Diego Mercerat and Josep de la Puente that helped us to improve the article.

REFERENCES

Belytschko, T., Liu, W.K. & Moran, B., 2000. *Nonlinear Finite Elements for Continua and Structures,* John Wiley & Sons, New York, NY.

Bielak J., Loukakis, K., Hisada, Y. & Yoshimura, Ch., 2003. Domain reduction method for three-dimensional earthquake modeling in localized regions. Part I: theory, *Bull. seism. Soc. Am.,* **93,** 8170–824.

Chaljub, E., Komatitsch, D., Vilotte, J.-P., Capdeville, Y., Valette, B. & Festa, G., 2007. Spectral element analysis in seismology, in *Advances in Wave Propagation in Heterogeneous Earth,* Advances in Geophysics Series Vol. 48, pp. 365–419, eds Wu, R.-S. & Maupin, V., Elsevier–Academic Press, London.

Chaljub, E. *et al*. 2010a. Euroseistest Numerical Simulation Project: comparison with local earthquake recordings for validation, *Seismol. Res. Lett.,* **81,** 1427–1455.

Chaljub, E., Moczo, P., Tsuno, S., Bard, P.-Y., Kristek, J., Käser, M., Stupazzini, M., Kristekova, M., 2010b. Quantitative comparison of four numerical predictions of 3D ground: motion in the Grenoble Valley, France, *Bull. seism. Soc. Am.,* **100,** 1427–1455.

De Basabe, J.D. & Sen, M.K., 2007. Grid dispersion and stability criteria of some common finite-element methods for acoustic and elastic wave equations, *Geophysics,* **72,** T81–T95.

De Basabe, J.D., Sen, M.K. & Wheeler, M., 2008. The interior penalty discontinuous Galerkin method for elastic wave propagation: grid dispersion. *Geophys. J. Int.,* **175,** 83–93.

de la Puente, J., 2008. *Seismic Wave Propagation for Complex Rheologies,* VDM Verlag, Saarbrücken.

de la Puente, J., Dumbser, M., Käser, M. & Igel, H., 2008. Discontinuous Galerkin methods for wave propagation in poroelastic media, *Geophysics,* **73,** 77–97.

de la Puente, J., Käser, M., Dumbser, M. & Igel, H., 2007. An arbitrary high order discontinuous Galerkin method for elastic waves on unstructured meshes – IV. Anisotropy, *Geophys. J. Int.,* **169,** 1210–1228.

Delcourte, S., Fezoui, L. & Glinsky-Olivier, N., 2009. A high-order discontinuous Galerkin method for the seismic wave propagation, *ESAIM: Proc.,* **27,** 70–89.

Dumbser, M. & Käser, M., 2006. An arbitrary high order discontinuous Galerkin method for elastic waves on unstructured meshes – II. The three-dimensional case, *Geophys. J. Int.,* **167,** 319–336.

Dumbser, M., Käser, M. & Toro, E., 2007. An arbitrary high order discontinuous Galerkin method for elastic waves on unstructured meshes – V. Local time stepping and p-adaptivity, *Geophys. J. Int.,* **171,** 695–717.

Etienne, V., Chaljub, E., Virieux, J. & Glinsky, N., 2010. An hp-adaptive discontinuous Galerkin finite-element method for 3D elastic wave modelling, *Geophys. J. Int.,* **183,** 941–962.

Galis, M., Moczo, P. & Kristek, J., 2008. A 3-D hybrid finite-difference—finite-element viscoelastic modelling of seismic wave motion, *Geophys. J. Int.,* **175,** 153–184.

Hesthaven, J.S. & Warburton, T., 2008. Nodal discontinuous Galerkin Method, in *Algorithms, Analysis, and Application,* Springer, New York, NY.

Hughes, T.J.R., 2000. *The Finite Element Method: Linear Static and Dynamic Finite Element Method Analysis,* Prentice Hall, New York, NY.

Käser, M. & Dumbser, M., 2006. An arbitrary high order discontinuous Galerkin method for elastic waves on unstructured meshes – I. The two-dimensional isotropic case with external source terms, *Geophys. J. Int.,* **166,** 855–877.

Käser, M., Dumbser, M., de la Puente, J. & Igel, H., 2007. An arbitrary high order discontinuous Galerkin method for elastic waves on unstructured meshes – III. Viscoelastic attenuation, *Geophys. J. Int.,* **168,** 224–242.

Käser, M., Hermann, V. & de la Puente, J., 2008. Quantitative accuracy analysis of the discontinuous Galerkin method for seismic wave propagation, *Geophys. J. Int.,* **173,** 990–999.

Komatitsch, D. & Tromp, J., 1999. Introduction to the spectral element method for three-dimensional seismic wave propagation, *Geophys. J. Int.,* **139,** 806–822.

Komatitsch, D., Tsuboi, S. & Tromp, J., 2005. The spectral-element method in seismology, *Geophys. Monogr. Ser.*, **157**, 205–227.

Komatitsch, D. & Vilotte, J.-P., 1998. The spectral-element method: an efficient tool to simulate the seismic response of 2D and 3D geological structures, *Bull. seism. Soc. Am.,* **88,** 368–392.

LeVeque, R.J., 2002. *Finite Volume Methods For Hyperbolic Problems*.*Cambridge Texts in Applied Mathematics,* Cambridge University Press, Cambridge.

Ma, S. & Liu, P., 2006. Modeling of the perfectly matched layer absorbing boundaries and intrinsic attenuation in explicit finite-element methods, *Bull. seism. Soc. Am.,* **96,** 1779–1794.

Moczo, P. *et al*., 2010a. Numerical modeling of earthquake ground motion in the Mygdonian Basin, Greece: verification of the 3D numerical methods, *Seism. Res. Lett.,* **81,** 310.

Moczo, P., Kristek, J., Galis, M., Pazak, P., 2010b. On accuracy of the finite-difference and finite-element schemes with respect to P-wave to S-wave speed ratio, *Geophys. J. Int.,* **182,** 493–510.

Moczo, P., Kristek, J., Galis, M., Pazak, P. & Balazovjech, M., 2007a. The finite-difference and finite-element modeling of seismic wave propagation and earthquake motion, *Acta Phys. Slovaca,* **57,** 177–406.

Moczo, P., Kristek, J. & Halada, L., 2000. 3D 4th-order staggered-grid finite-difference schemes: stability and grid dispersion. *Bull. seism. Soc. Am.,* **90,** 587–603.

Moczo, P., Robertsson, J.O.A. & Eisner, L., 2007b. The finite-difference time-domain method for modeling of seismic wave propagation, in *Advances in Wave Propagation in Heterogeneous Earth,* Advances in Geophysics Series Vol. 48, pp. 421–516, eds Wu, R.-S., Maupin, V. & Dmowska, R., Elsevier/Academic Press, San Diego, CA.

Ottosen, N.S. & Petersson, H., 1992. *Introduction to the Finite Element Method,* Prentice Hall, New York, NY.

Reddy, J.N., 2006. *An Introduction to the Finite Element Method,* McGraw-Hill, New York, NY.

Seriani, G. & Oliveira, S.P., 2008. Dispersion analysis of spectral element methods for elastic wave propagation, *Wave Motion* **45,** 729–744.

Zienkiewicz, O.C. & Taylor, R.L., 1989. *The Finite Element Method,* 4th edn, Vol. 1, McGraw-Hill, New York, NY.

APPENDIX

Table A1. The leading and first higher terms of the truncation errors of the non-mixed and mixed spatial operators defined by eqs (11)–(14). Part a: second-order operators, part b: fourth-order operators.

Operator	Truncation error × 20160
Part (a)	
$D_{xx}^{\text{FD D CG 2}}$ $D_{xx}^{\text{FE L8}}$ $D_{xx}^{\text{DG P0 CF}}$	$1680\,\Psi^{(4,0,0)}\,h^2$ $+\,56\,\Psi^{(6,0,0)}\,h^4$
$D_{zx}^{\text{FD D CG 2}}$ $D_{zx}^{\text{FE L8}}$ $D_{zx}^{\text{DG P0 CF}}$	$6720\left(\frac{1}{2}\Psi^{(1,0,3)}+\frac{1}{2}\Psi^{(3,0,1)}\right)h^2$ $+\,896\left(\frac{3}{16}\Psi^{(1,0,5)}+\frac{10}{16}\Psi^{(3,0,3)}+\frac{3}{16}\Psi^{(5,0,1)}\right)h^4$
$D_{xx}^{\text{FD DS PSG 2}}$ $D_{xx}^{\text{FE G1}}$	$11760\left(\frac{3}{7}\Psi^{(2,0,2)}+\frac{1}{7}\Psi^{(4,0,0)}+\frac{3}{7}\Psi^{(2,2,0)}\right)h^2$ $+\,2996\left(\frac{1}{107}\left(2\Psi^{(6,0,0)}+15\Psi^{(4,2,0)}+15\Psi^{(4,0,2)}+15\Psi^{(2,4,0)}+45\Psi^{(2,2,2)}+15\Psi^{(2,0,4)}\right)\right)h^4$
$D_{zx}^{\text{FD DS PSG 2}}$ $D_{zx}^{\text{FE G1}}$	$11760\left(\frac{2}{7}\Psi^{(1,0,3)}+\frac{3}{7}\Psi^{(1,2,1)}+\frac{2}{7}\Psi^{(3,0,1)}\right)h^2$ $+\,2996\left(\frac{1}{107}\left(6\Psi^{(1,0,5)}+30\Psi^{(1,2,3)}+15\Psi^{(1,4,1)}+20\Psi^{(3,0,3)}+30\Psi^{(3,2,1)}+6\Psi^{(5,0,1)}\right)\right)h^4$

Table A1. (*Continued.*)

Operator	Truncation error × 20160
$D_{xx}^{\text{FD DS SG 2}}$	$1680\ \Psi^{(4,0,0)}\ h^2$
	$+ 56\ \Psi^{(6,0,0)}\ h^4$
$D_{zx}^{\text{FD DS SG 2}}$	$1680\ \left(\frac{1}{2}\Psi^{(1,0,3)} + \frac{1}{2}\Psi^{(3,0,1)}\right)\ h^2$
	$+ 56\ \left(\frac{3}{16}\Psi^{(1,0,5)} + \frac{10}{16}\Psi^{(3,0,3)} + \frac{3}{16}\Psi^{(5,0,1)}\right)\ h^4$
$D_{xx}^{\text{FE G8}}$	$8400\ \left(\frac{2}{5}\Psi^{(2,0,2)} + \frac{1}{5}\Psi^{(4,0,0)} + \frac{2}{5}\Psi^{(2,2,0)}\right)\ h^2$
$D_{xx}^{\text{DG P1 CF}}$	$+ 1736\ \left(\frac{1}{31}\left(\Psi^{(6,0,0)} + 5\Psi^{(4,2,0)} + 5\Psi^{(4,0,2)} + 5\Psi^{(2,4,0)} + 10\Psi^{(2,2,2)} + 5\Psi^{(2,0,4)}\right)\right)\ h^4$
$D_{zx}^{\text{FE G8}}$	$10080\ \left(\frac{1}{3}\Psi^{(1,0,3)} + \frac{1}{3}\Psi^{(1,2,1)} + \frac{1}{3}\Psi^{(3,0,1)}\right)\ h^2$
$D_{zx}^{\text{DG P1 CF}}$	$+ 2996\ \left(\frac{1}{41}\left(3\Psi^{(1,0,5)} + 10\Psi^{(1,2,3)} + 5\Psi^{(1,4,1)} + 10\Psi^{(3,0,3)} + 10\Psi^{(3,2,1)} + 3\Psi^{(5,0,1)}\right)\right)\ h^4$
Part (b)	
$D_{xx}^{\text{FD D CG 4}a}$	$- 1344\ \Psi^{(6,0,0)}\ h^4$
	$- 300\ \Psi^{(8,0,0)}\ h^6$
$D_{zx}^{\text{FD D CG 4}a}$	$- 1344\ \left(\frac{1}{2}\Psi^{(1,0,5)} + \frac{1}{2}\Psi^{(5,0,1)}\right)\ h^4$
	$- 160\ \left(\frac{1}{2}\Psi^{(1,0,7)} + \frac{1}{2}\Psi^{(7,0,1)}\right)\ h^6$
$D_{xx}^{\text{FD D CG 4b}}$	$- 224\ \Psi^{(6,0,0)}\ h^4$
	$- 20\ \Psi^{(8,0,0)}\ h^6$
$D_{zx}^{\text{FD D CG 4b}}$	$- 1904\ \left(\frac{6}{17}\Psi^{(1,0,5)} + \frac{5}{17}\Psi^{(3,0,3)} + \frac{6}{17}\Psi^{(5,0,1)}\right)\ h^4$
	$- 440\ \left(\frac{4}{22}\Psi^{(1,0,7)} + \frac{7}{22}\Psi^{(3,0,5)} + \frac{7}{22}\Psi^{(5,0,3)} + \frac{4}{22}\Psi^{(7,0,1)}\right)\ h^6$
$D_{xx}^{\text{FD DS SG 4}}$	$- 189\ \Psi^{(6,0,0)}\ h^4$
	$- \frac{45}{4}\ \Psi^{(8,0,0)}\ h^6$
$D_{zx}^{\text{FD DS SG 4}}$	$- 189\ \left(\frac{1}{2}\Psi^{(1,0,5)} + \frac{1}{2}\Psi^{(5,0,1)}\right)\ h^4$
	$- \frac{45}{4}\ \left(\frac{1}{2}\Psi^{(1,0,7)} + \frac{1}{2}\Psi^{(7,0,1)}\right)\ h^6$
$D_{xx}^{\text{SE 4 cn}}$	$- 384\ \Psi^{(6,0,0)}\ h^4$
	$-\frac{1920}{49}\ \Psi^{(8,0,0)}\ h^6$
$D_{zx}^{\text{SE 4 cn}}$	$- 2304\ \left(\frac{1}{2}\Psi^{(1,0,5)} + \frac{1}{2}\Psi^{(5,0,1)}\right)\ h^4$
	$- \frac{15\,360}{49}\ \left(\frac{1}{2}\Psi^{(1,0,7)} + \frac{1}{2}\Psi^{(7,0,1)}\right)\ h^6$
$D_{xx}^{\text{SE 4 vn}}$	$- 1\,024\ \Psi^{(6,0,0)}\ h^4$
	$- \frac{58\,880}{49}\ \Psi^{(8,0,0)}\ h^6$
$D_{zx}^{\text{SE 4 vn}}$	$- 6144\ \left(\frac{1}{2}\Psi^{(1,0,5)} + \frac{1}{2}\Psi^{(5,0,1)}\right)\ h^4$
	$- \frac{471\,040}{49}\ \left(\frac{1}{2}\Psi^{(1,0,7)} + \frac{1}{2}\Psi^{(7,0,1)}\right)\ h^6$